Search for compressed mass Higgsino production with soft lepton tracks with the CMS experiment in proton-proton collision data at $\sqrt{s} = 13$ TeV

VORGELEGT VON

Yuval Nissan

IM August 2022

Universität Hamburg

DER FORSCHUNG | DER LEHRE | DER BILDUNG

Abstract This is the abstract

Contents

Chapter 1

Introduction

This is a line in introduction. This is the introduction to the thesis.

Chapter 2

Quantum Field Theory and The Standard Model

2.1 Quantum Field Theory

2.2 The Standard Model of particle physics

2.2.1 The particle content

Chapter 3

Supersymmetry

3.0.1 Phenomenology of Higgsino production

Chapter 4

Multivariate Statistics

4.1 Decision Trees

Chapter 5

Experimental setup: Collider, detector, and algorithms

Chapter 6

Search for compressed Higgsinos with soft lepton tracks

6.1 Motivation

6.2 Previous searches

6.3 Signal models

The signal models considered in this analysis are based on **FiXme Note: fill in signal model stuff**.
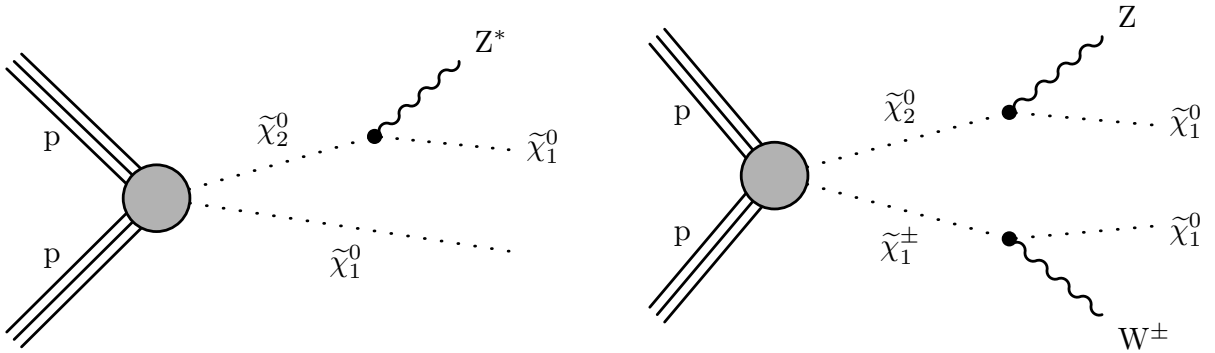

Figure 6.1: Production and decay of electroweakinos in the higgsino simplified model through $\widetilde{\chi}_2^0 \, \widetilde{\chi}_1^0$ (left) and $\widetilde{\chi}_2^0 \, \widetilde{\chi}_1^\pm$ (right).

6.4   Signal signature and base selection

To build an effective analysis strategy, the signal kinematics must be studied and exploited. The electroweakino production in question exhibit unique features which can be used in order to discriminate between the signal and the Standard Model (SM) background. It is important to explore these signal distributions in order to define a preselection, or a base cut, that will serve the purpose of retaining as much signal as possible while rejecting as much background. All of the following distributions were plotted by weighting the simulation to Run II luminosity of $\mathcal{L} = 135 \, \text{fb}^{-1}$ and requiring at least one jet in the event with $p_\text{T} \geq 30 \, \text{GeV}$ and $|\eta| < 2.4$. Further selection might apply and will be listed in each section in that case.

6.4.1   Missing Transverse Energy

One property that essentially all Dark Matter (DM) searches have in common is the presence of a DM candidate in the production. The exact identity and properties of said particle (or particles in the case multiple DM candidates) vary, but they do share a lot in common. The DM candidate in our Supersymmetry (SUSY) search is the neutralino, which is a type of DM candidate referred to as a Weakly Interacting Massive Particle (WIMP). A WIMP, broadly speaking, is a new elementary particle which interacts via gravity and any other force (or forces), potentially not part of the SM itself, which is as weak as or weaker than the weak nuclear force, but also non-vanishing in its strength. That essentially means that such candidate is neutral, and therefore not interacting via the electromagnetic force. A neutral particle that interacts neither electromagnetically nor via the strong force (i.e. colorless) will escape detection and will leave traces in the form of a transverse momentum imbalance, which we refer to as E_T^miss (Missing Transverse Energy or Missing Transverse Momentum). Our signal contains two DM candidates in the production, which are the Lightest SUSY Particles (LSPs), the neutralinos $\widetilde{\chi}_1^0$. We therefore expect the signal to contain considerable magnitude of E_T^miss. As described in 6.7.4, **FiXme Note: make sure we described both met and mht** we are more interesting in H_T^miss, which is highly correlated with E_T^miss, due to our definition of lepton isolation and its use in the background estimation methods. Nonetheless, we will look at both E_T^miss and H_T^miss observables. **FiXme Note: make sure we define the different deltaM somewhere**

As we expect, E_T^miss and H_T^miss are hardly affected by the different choices for Δm, while the higgsino parameter μ affect the distributions above all through its lower production cross section for higher higgsino parameter μ. As discuss at 6.8, the region of interest lie at $H_\text{T}^\text{miss} \geq 220$ for triggering purposes. Even though this is quite a harsh and inefficient cut, one must look also at the SM background at the regions of $H_\text{T}^\text{miss} < 220$ and $H_\text{T}^\text{miss} \geq 220$ to conclude that most of the sensitivity comes from the $H_\text{T}^\text{miss} \geq 220$ region, since the production of real H_T^miss (or E_T^miss) result from the production of neutrinos in the event, and these are much less common than Quantum Chromodynamics (QCD) events which swarm the $H_\text{T}^\text{miss} < 220$ region. Therefore, cutting at $H_\text{T}^\text{miss} \geq 220$ might be inefficient, but results in high sensitivity.

6.4.2   Jets and hardronic activity

Since the neutralinos $\widetilde{\chi}_1^0$ escaping the detector are the contributors to the H_T^miss and in doing so the drivers of the sensitivity in high H_T^miss region, we want them to be as boosted as possible, i.e., with the highest transverse momentum p_T as possible. A widely used approach is to require **FiXme Note: add citation** an Initial State Radiation (ISR) jet in the event. An ISR jet is formed when one of the incoming protons emit radiation (such as a photon or a gluon) before the interaction **FiXme Note: add citation and maybe reference to other section**. If a
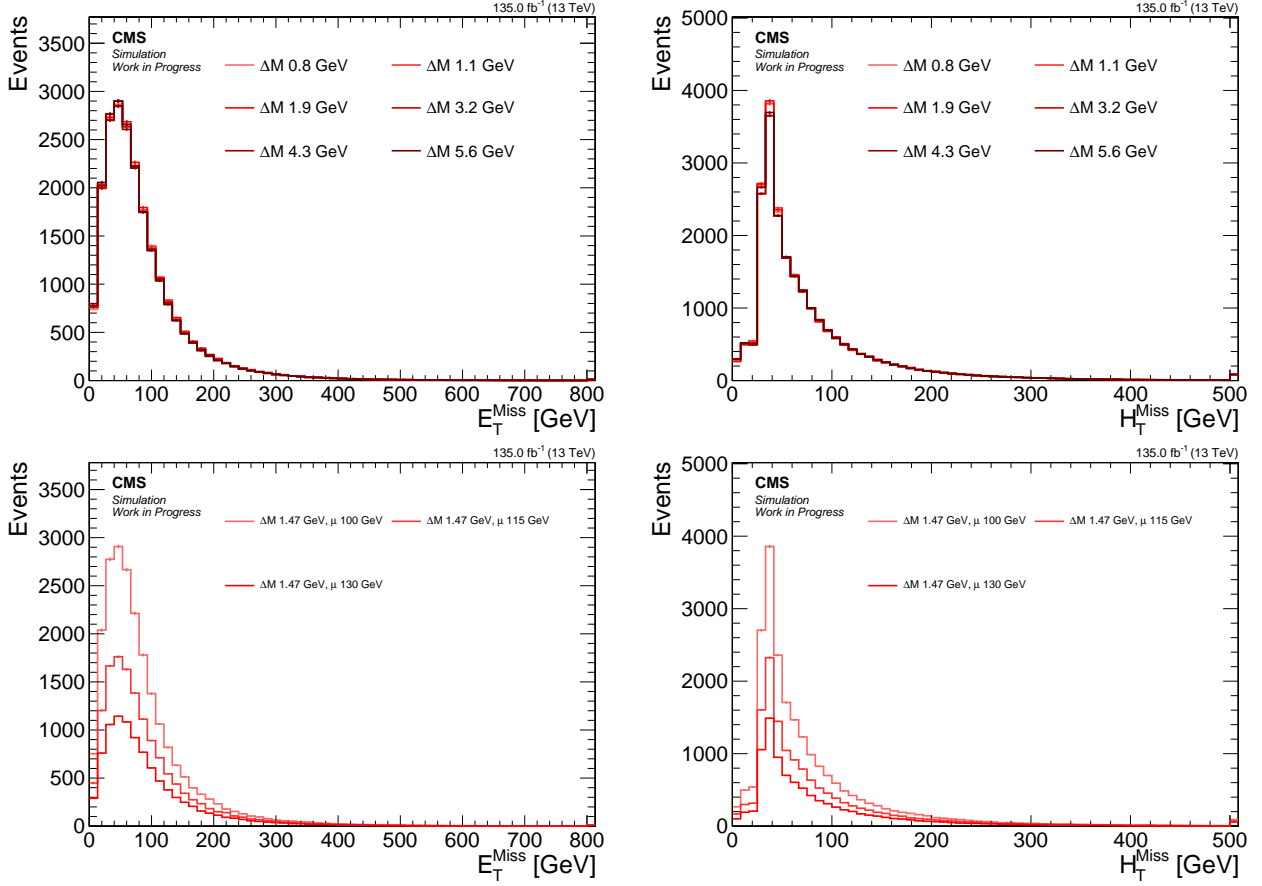
Figure 6.2: Signal distributions for E_T^{miss} (left) and H_T^{miss} (right) comparing various Δm with a fixed higgsino parameter $\mu = 100\,\text{GeV}$ (upper), and comparing various higgsino parameters μ with fixed Δm $= 1.47\,\text{GeV}$ (lower).

jet with high enough p_T is emitted, the rest of the interaction is recoiled against this jet and boosting it in the other direction. This way, the boosted neutralinos $\tilde{\chi}_1^0$ will result in higher H_T^{miss}. As described in **FiXme Note: ref**, we require the jets to have $p_T \geq 30\,\text{GeV}$ and be located within the tracker acceptance ($|\eta| < 2.4$). We require at least one such jet in the event.

Our signal signature does not include a b-jet, i.e., a jet resulting from a bottom quark hadronization (either resulting from a top quark or not). We therefore seek to exploit this knowledge by vetoing b-tagged jets in the event. As described in **FiXme Note: add ref** we are using DeepCSV flavor tagging discriminant with a medium working point. As can be seen in these distributions, most of the signal lie in the 0 bin, and we will therefore veto any b-tagged jet, which retains most of the signal, but rejects a lot of SM background, such as arising from $t\bar{t}$ events.

Since we are requiring an ISR jet in the event, we expect the E_T^{miss} and the H_T^{miss} to point in the opposite direction of the jet, or at least in an angel close to π. Events with multiple jets in the SM background such as arising from QCD will not exhibit such a feature. In order to reduce QCD background, we require min $\Delta\phi\left(H_T^{\text{miss}}, \text{jets}\right) > 0.4$.

6.4.3 Base selection

We recap the section by summarizing the base selection of our analysis. This base selection, or preselection as we might use call it interchangeably, is applied to all analysis categories.
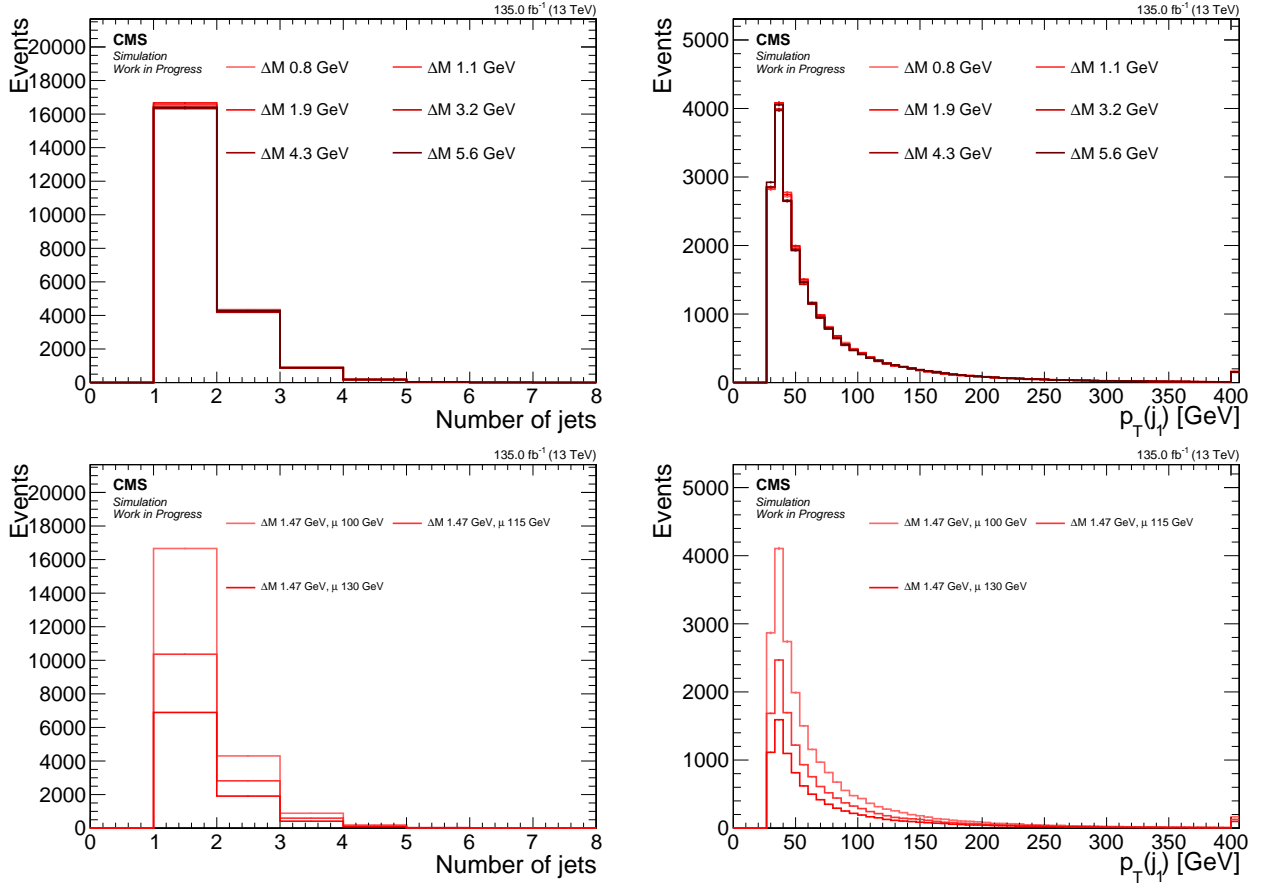
Figure 6.3:   Signal distributions for *number of jets* (left) and *leading jet* p_{T} (right) comparing various Δm with a fixed higgsino parameter $\mu = 100\,\mathrm{GeV}$ (upper), and comparing various higgsino parameters μ with fixed Δm $= 1.47\,\mathrm{GeV}$ (lower).

Figure 6.4:   Signal distributions for *number of b-tagged jets* comparing various Δm with a fixed higgsino parameter $\mu = 100\,\mathrm{GeV}$ (left), and comparing various higgsino parameters μ with fixed Δm $= 1.47\,\mathrm{GeV}$ (right).

6.4.4   Dilepton kinematics

Thus far we have looked at kinematic distributions ignoring the leptons in event. However, the most distinct features of the signal lie in the dilepton system. To fully understand the unique phase space of the dilepton system, we first look at generator level distributions and then look at what effects does reconstruction have on those observables. In addition, since the most sensitive category is the dimuon category due to its much lower threshold on the

Figure 6.5: Signal distributions for $\min \Delta\phi\left(E_{\mathrm{T}}^{\mathrm{miss}}, \mathrm{jets}\right)$ (left) and $\min \Delta\phi\left(H_{\mathrm{T}}^{\mathrm{miss}}, \mathrm{jets}\right)$ (right) comparing various Δm with a fixed higgsino parameter $\mu = 100\,\mathrm{GeV}$ (upper), and comparing various higgsino parameters μ with fixed $\Delta m = 1.47\,\mathrm{GeV}$ (lower).
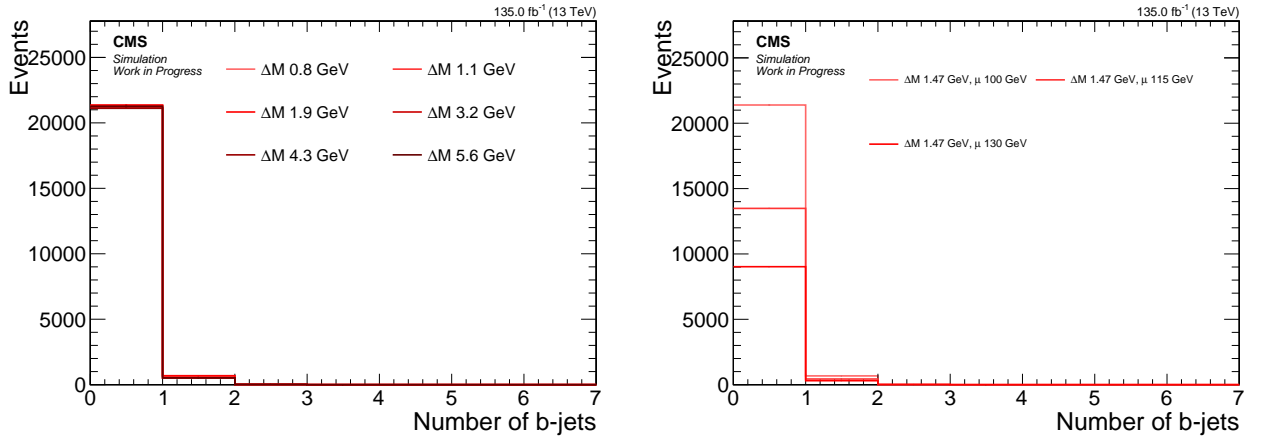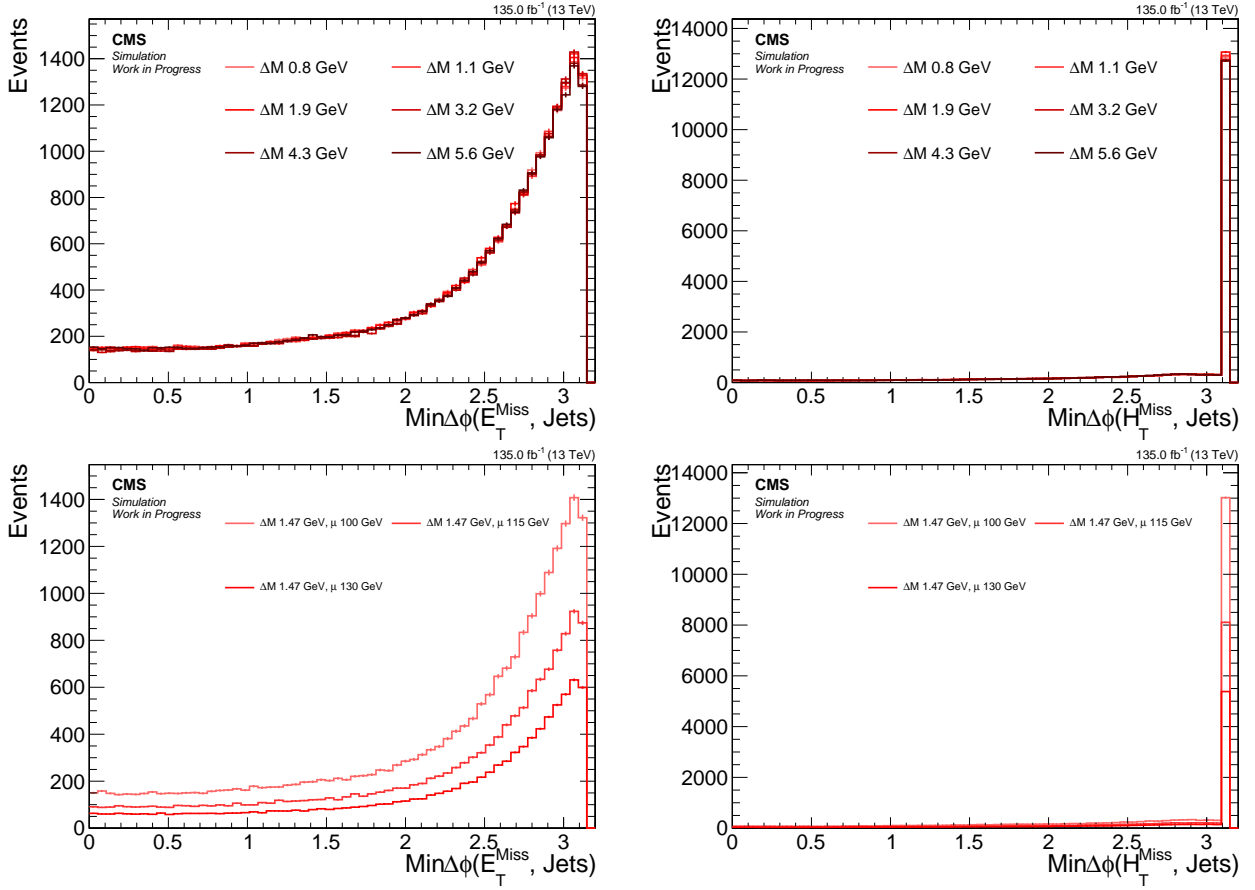
Table 6.1: Base selection applied to all analysis categories

Variable	Value
$H_{\mathrm{T}}^{\mathrm{miss}}\,[\,\mathrm{GeV}]$	≥ 220
$N_{\mathrm{jets}}\left(p_{\mathrm{T}} \geq 30\,\mathrm{GeV}\text{ and }|\eta| < 2.4\right)$	≥ 1
$N_{\mathrm{b-jets}}\left(p_{\mathrm{T}} \geq 30\,\mathrm{GeV}\text{ and }|\eta| < 2.4\right)$	0
$\min \Delta\phi\left(H_{\mathrm{T}}^{\mathrm{miss}}, \mathrm{jets}\right)$	> 0.4

transverse momentum, these events are shown in the following sections, leaving the events with two electrons to the appendix **FiXme Note: ref**.

Since the kinematics changes dramatically as a function of Δm, but changes almost only in overall normalization due to the production cross section as a function of the higgsino parameter μ, in the following sections, we set the higgsino parameter to $\mu = 100\,\mathrm{GeV}$ and vary the Δm.

Lepton η and transverse momentum p_{T}

The transverse momentum p_{T} distribution of the muons and our access to a subset of its full range, have dramatic effect on the signal acceptance and the sensitivity. The muon reconstruction process and details are discussed in **FiXme Note: ref**. The selection we apply to the muons in this analysis is described in 6.7.2 and will be referred to here as *analysis selection*. In this section we would like to consider specifically the importance of the p_{T} on the signal and its dilepton kinematic distributions.

We begin by having a look at the generator level distribution of p_T, or in other words, the so-called *truth* distributions, which do not exhibit any detector or reconstruction features, and compare to the reconstructed distribution.
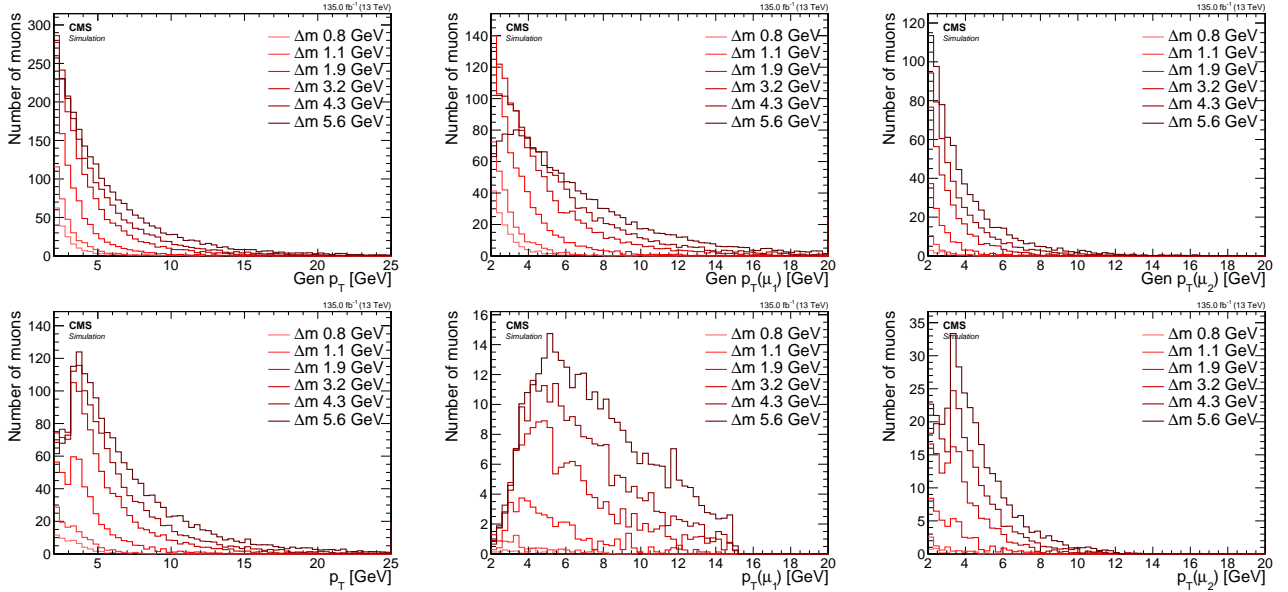

Figure 6.6: Signal p_T distributions for inclusive (left), leading muon μ_1 (middle), subleading muon μ_2 (right) at generator level (top) and reconstruction level passing analysis selection (bottom).

By comparing the generator level to the reconstruction level of the inclusive p_T distribution, we see that a reshaping occurs at around 3 GeV. A significant portion of the generated muons with $p_\mathrm{T} < 3$ GeV are being lost in reconstruction. The reconstructed subleading p_T distribution has a camel shape whereby the efficiency drops bellow p_T of 3 GeV and only partially regained at $p_\mathrm{T} < 3$ GeV. This is a detector effect and can be seen more clearly when we split the p_T distribution into a barrel ($|\eta| < 1.2$) and encaps ($|\eta| \geq 1.2$) portions.

The picture becomes much clearer in regards to the reconstruction efficiency as a function of p_T. When comparing the generator level distribution of the barrel muons on the top left with its constructed counterpart on the bottom left, we see that the barrel is almost completely unable to reconstruct muons with $p_\mathrm{T} < 3$ GeV, while the endcaps, shown on the left, are able to do so. As we will see in the $m_{\ell\ell}$ and ΔR upcoming sections (6.4.4 and 6.4.4), since those distribution have an important relationship, that has consequences in regards to reshaping kinematic distributions, as well as signal acceptance in general. Since the low region of $2 \leq p_\mathrm{T} \leq 3.5$ GeV is crucial in giving us access to low Δm signal points, it is achieved, as can be seen here, mainly with the help of the muon chamber endcaps.

Since the barrel and endcaps are seperated by different regions of η, $|\eta| < 1.2$ for barrel and $|\eta| \geq 1.2$ for endcaps, it worth taking a look at the η distributions of the muons as well.

Our muons analysis selection picks only muons in the tracker range of $|\eta| < 2.4$ which is the reason why the reconstruction plots on the bottom do not have muons with $|eta| > 2.4$. We see that the main effect going from the inclusive $|\eta|$ in generator level to the reconstructed counter part, is the flattening of the distribution due to the loss of muons with $|eta| < 1.2$ in the barrel for muons with $p_\mathrm{T} < 3$ GeV.

With the understanding of the reconstruction effects on the p_T and η distributions of the muons, we are equipped to look further into other kinematic variables of the dilepton system.
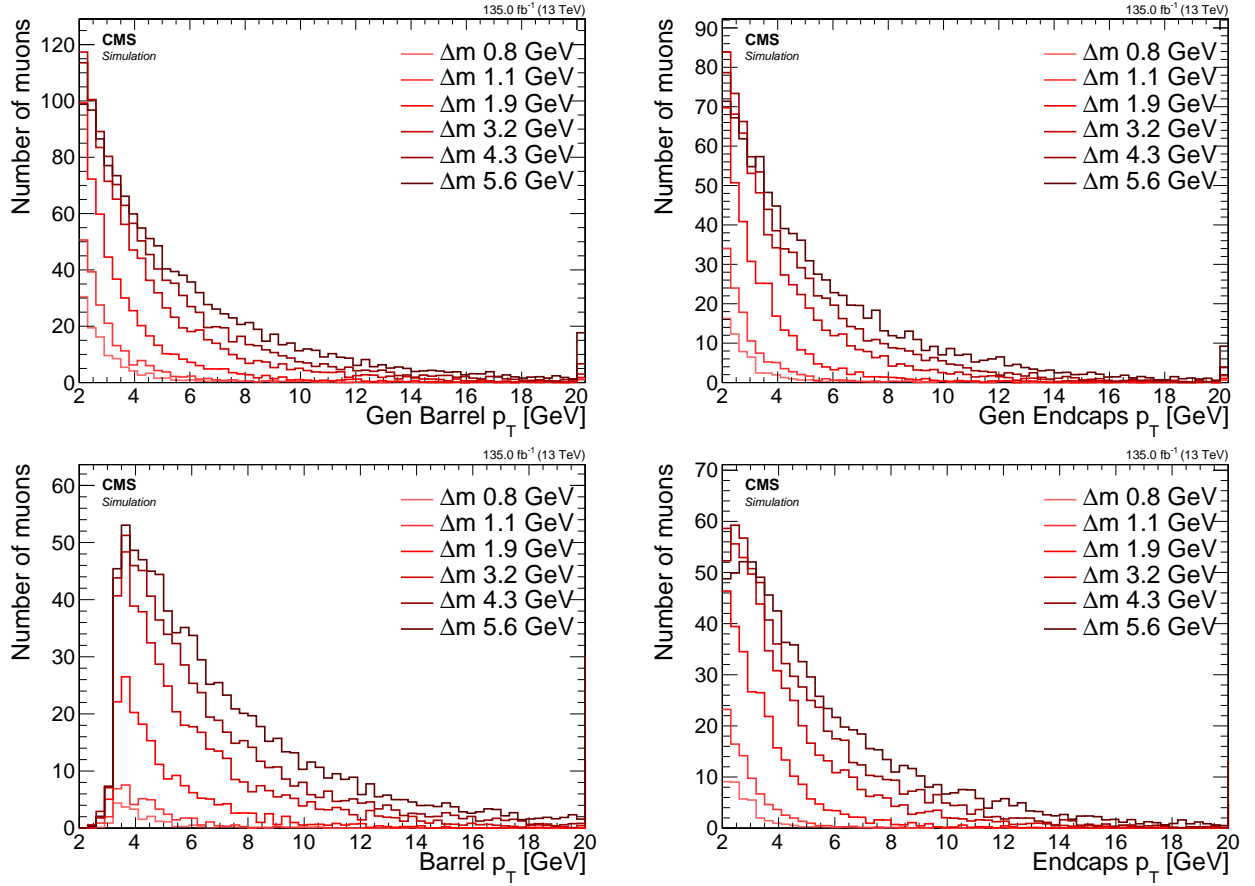
Figure 6.7: Signal inclusive p_T distributions for barrel $|\eta| < 1.2$ (left) and endcaps $|\eta| \geq 1.2$ (right) at generator level (top) and reconstruction level passing analysis selection (bottom).
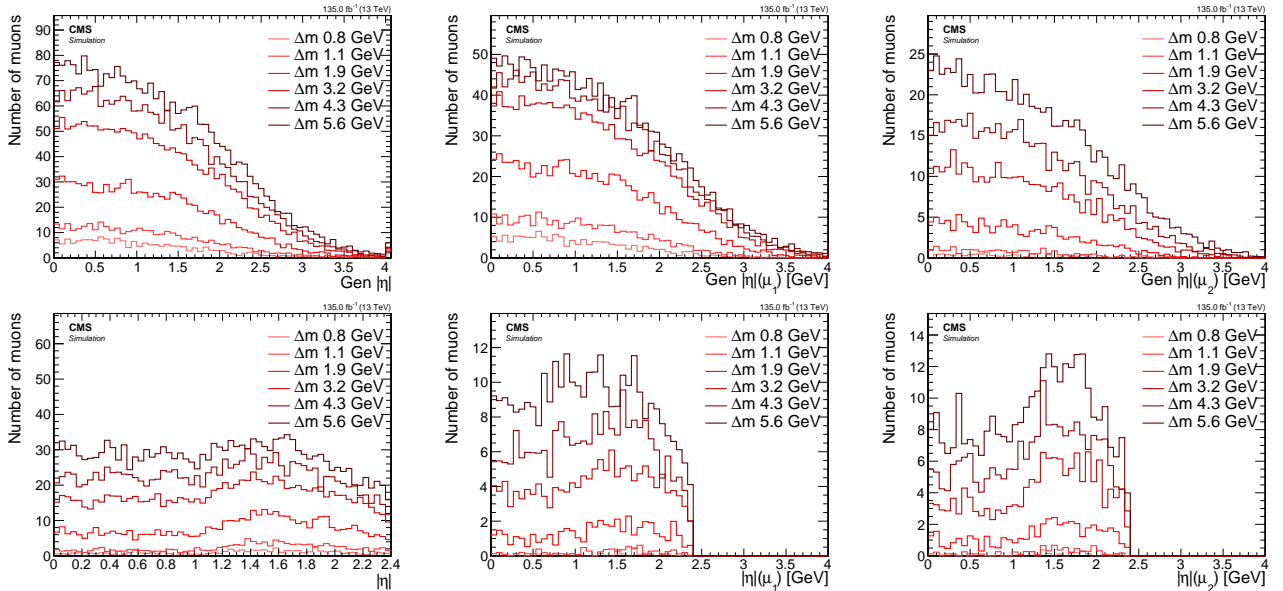

Figure 6.8: Signal $|\eta|$ distributions for inclusive (left), leading muon μ_1 (middle), subleading muon μ_2 (right) at generator level (top) and reconstruction level passing analysis selection (bottom).

Invariant mass $m_{\ell\ell}$

The invariant mass of the two leptons that result from the decay of the $\widetilde{\chi}_2^0$ has a unique shape due to the limited allowed phase space of the leptons as part of the 3-body decay. Since the $\widetilde{\chi}_2^0$

decays into $\widetilde{\chi}_1^0$ and $\ell^+\ell^-$ through a Z^*, the allowed phase space of the dilepton pair is restricted to the mass difference between $\widetilde{\chi}_2^0$ and $\widetilde{\chi}_1^0$, i.e., Δm. We therefore expect the $m_{\ell\ell}$ distribution to have an edge at Δm.
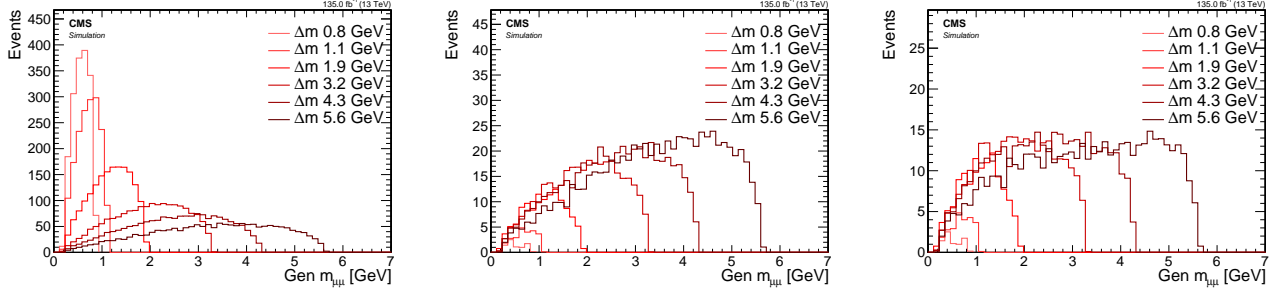

Figure 6.9: Signal generator level $m_{\ell\ell}$ distributions with no cuts (left), with $p_{\mathrm{T}}\left(\mu_i\right) >$ $2\,\mathrm{GeV}$, $i = 1, 2$ (middle) and with SOS orthogonality condition $p_{\mathrm{T}}\left(\mu_i\right) > 2\,\mathrm{GeV}$, $p_{\mathrm{T}}\left(\mu_2\right) \leq 3.5\,\mathrm{GeV}$ or $\Delta R \leq 0.3$ (right).

We see the original invariant mass of the muons $m_{\mu\mu}$ on the left. For each signal point, the edge of the $m_{\mu\mu}$ distribution is right at the corresponding Δm. However, once we cut on the muons p_{T} and require $p_{\mathrm{T}} \geq 2\,\mathrm{GeV}$, the shape shifts, and the efficiency in the lower Δm drops dramatically, as can be seen from the middle plot. Lastly, the effect of orthogonalizing phase space to the SOS analysis can be seen on the right most plot. The effect is strongest in high Δm and quite subtle in low Δm.

To understand the reshaping that happens to the $m_{\mu\mu}$ shape, we look at the relationship between the p_{T} of the muons (leading muon denoted μ_1 while subleading muon is denoted μ_2) and the invariant mass one a signal with low Δm of $1.13\,\mathrm{GeV}$ and one with high Δm of $5.63\,\mathrm{GeV}$.

We have established earlier that the invariant mass distribution has an edge at the Δm and one can read the value of Δm from these plots. Another interesting feature to notice in these plots is that there is also a lower edge in the Δm distribution at around $\sim 0.2\,\mathrm{GeV}$ and that is of course due to each muon having a mass of around $\sim 0.1\,\mathrm{GeV}$. We can clearly see now that by cutting on both muons at $p_{\mathrm{T}} \geq 2\,\mathrm{GeV}$, we are loosing a lot of the signal. This effect, in fact, becomes quite substantial for the low Δm $= 1.13\,\mathrm{GeV}$ (top row). We quantify this effect by making a cutflow table where each row represents a cut, and its efficiency is calculated by dividing the number of events passing the cut by the number of events in the line before it. The first line is our baseline of all dimuon events with at least one jet with $p_{\mathrm{T}} \geq 30\,\mathrm{GeV}$ and $|\eta| < 2.4$ and has an efficiency of 1 by definition. The event number is weighted to Run II luminosity of $\mathcal{L} = 135\,\mathrm{fb}^{-1}$.

Table 6.2: Generator level efficiency on muons selections

Cut	Number of events		Efficiency	
	Δm $= 1.13\,\mathrm{GeV}$	Δm $= 5.63\,\mathrm{GeV}$	Δm $= 1.13\,\mathrm{GeV}$	Δm $= 5.63\,\mathrm{GeV}$
Baseline	1710.7	1743.9	1	1
$p_{\mathrm{T}} \geq 2\,\mathrm{GeV}$	24.7	724.9	0.015	0.41
SOS orthogonality	24.7	490.6	1	0.68

We observe that for the low Δm of $1.13\,\mathrm{GeV}$ the cut of $p_{\mathrm{T}} \geq 2\,\mathrm{GeV}$ is really hurting the acceptance of the signal with only 1.5% of signal remaining. In contrast, the orthogonality condition of requiring $p_{\mathrm{T}}\left(\mu_2\right) \leq 3.5\,\mathrm{GeV}$ or $\Delta R\left(\ell\ell\right) \leq 0.3$ is not effecting it any further. The picture is different for the high Δm of $5.63\,\mathrm{GeV}$ where the p_{T} cut is cutting away more than half of the signal and the SOS orthogonality an additional two thirds.
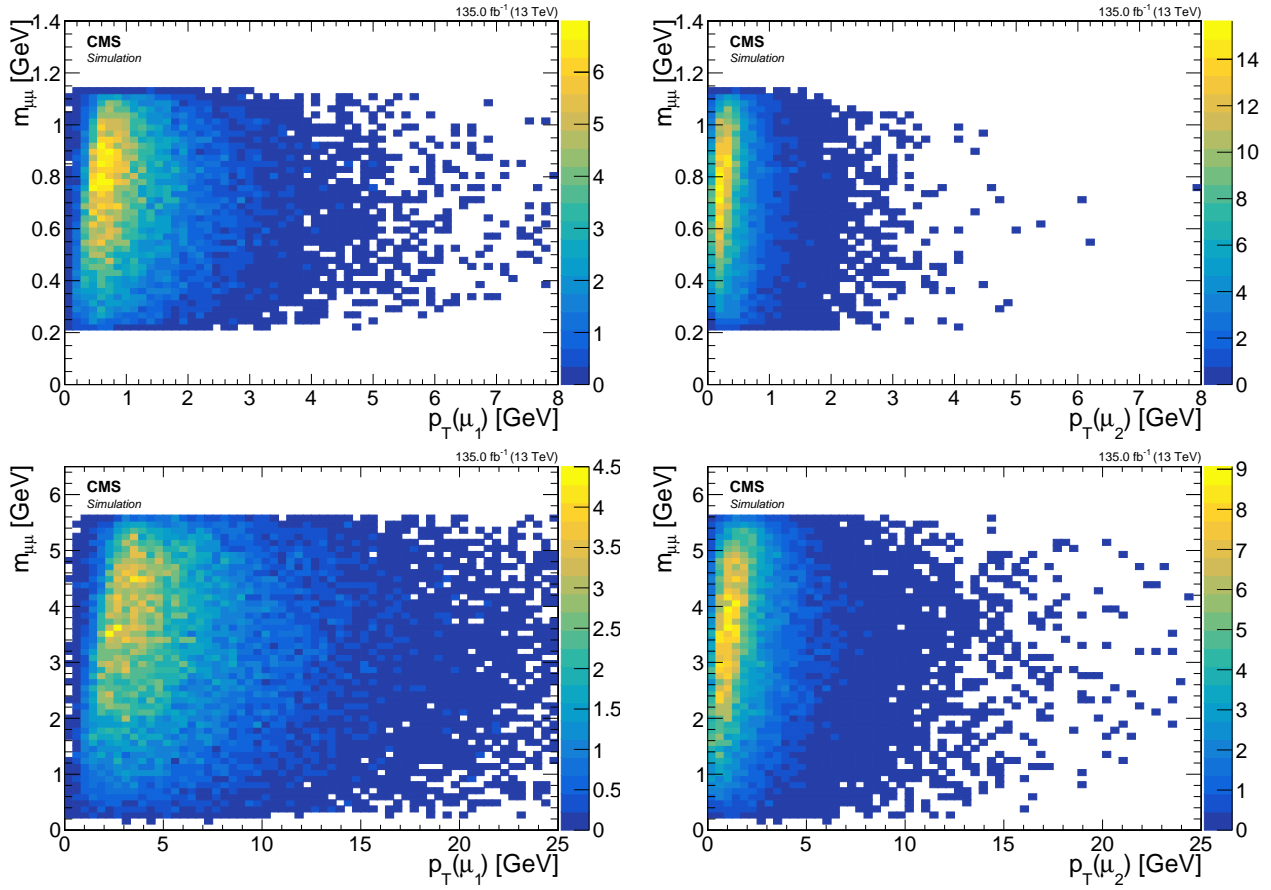
Figure 6.10: Signal $m_{\mu\mu}$ vs. p_{T} for leading lepton μ_1 (left) and subleading lepton μ_2 (right) for $\Delta\mathrm{m} = 1.13\,\mathrm{GeV}$ (top) and $\Delta\mathrm{m} = 5.63\,\mathrm{GeV}$ (bottom).

Since we have just established that due to the relationship between p_{T} and $m_{\ell\ell}$, the p_{T} distribution directly effects $m_{\ell\ell}$, we should also have a look at how to reconstruction effects discussed at 6.4.4 might effect the $m_{\mu\mu}$ distribution as well.
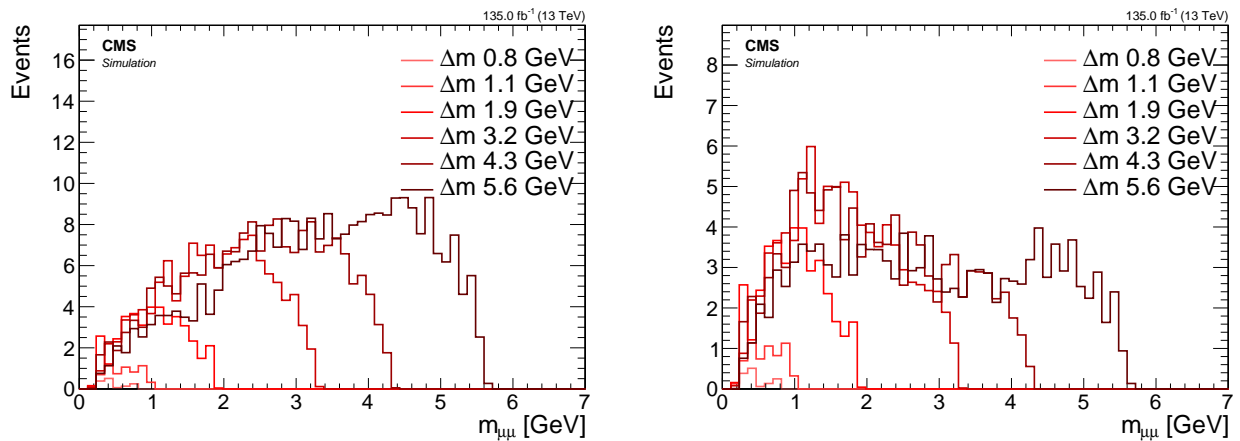

Figure 6.11: Signal reconstructed $m_{\mu\mu}$ with basic analysis selection (left) and additional SOS orthogonality condition (right).

It's interesting to compare these distributions to the two right ones in the generator level version at 6.9. We see that not only less events survive the reconstruction, but also that some $\Delta\mathrm{m}$ model points peak between $1\,\mathrm{GeV}$ to $2\,\mathrm{GeV}$ with SOS orthogonality condition applied. The reconstruction and selection efficiency is discussed in more details in **FiXme Note: ref**.

Lepton separation ΔR

The lepton separation is defined by $\Delta R = \sqrt{(\Delta\eta)^2 + (\Delta\phi)^2}$ where η is the pseudorapidity and ϕ is the azimuthal angle measured in radians. ΔR plays a major role in this analysis since the leptons tend to be produced in proximity to each other and thus to defy standard definitions of isolation. Special care is taken to ensure that the collimated nature of the leptons can still be used to distinguish the otherwise isolated leptons in the signal from the non-isolated leptons in the SM background. An additional point of interest is with respect to previous SOS analysis **FiXme Note: cite** that had a requirement of $\Delta R(\ell\ell) > 0.3$ which we attempt to revert here for orthogonality purposes.

In similar fashion to the invariant mass in 6.4.4, we look at distributions of ΔR for various choices of Δm with different cuts applied, and observe their effect.
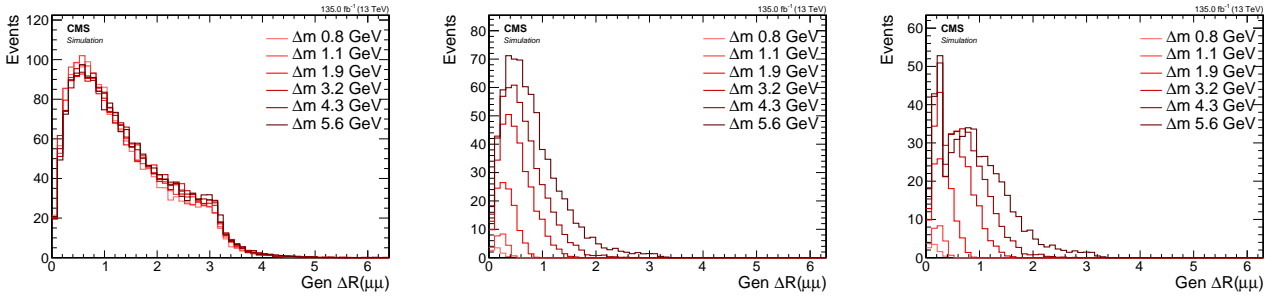

Figure 6.12: Signal generator level ΔR distributions with no cuts (left), with $p_{\mathrm{T}}(\mu_i) > 2\,\mathrm{GeV}$, $i = 1, 2$ (middle) and with SOS orthogonality condition $p_{\mathrm{T}}(\mu_i) > 2\,\mathrm{GeV}$, $p_{\mathrm{T}}(\mu_2) \leq 3.5\,\mathrm{GeV}$ or $\Delta R \leq 0.3$ (right).

As can be seen on the left plot, roughly the same amount of events are produced for all Δm model points, but when applying a cut of $p_{\mathrm{T}}(\mu) > 2\,\mathrm{GeV}$, a hierarchy of Δm points forms, with less events as Δm becomes smaller (middle plot). The spike on the right plot is due to the SOS orthogonality condition which requires $\Delta R(\ell\ell) \leq 0.3$ as one of two conditions in an or statement. To understand the shaping and hierarchy formation due to the p_{T} cut, we repeat the trick from the $m_{\mu\mu}$ in 6.4.4 and plot the p_{T} of the muons *vs.* $\Delta R(\ell\ell)$.

Now the hierarchy can be understood by observing that for Δm $= 1.13\,\mathrm{GeV}$, cutting $p_{\mathrm{T}}(\mu_2) \geq 2\,\mathrm{GeV}$ will limit the range of $\Delta R(\mu\mu)$ to less than 0.4 while leaving quite a large range exceeding 3 for the Δm $= 5.63\,\mathrm{GeV}$ model point.

We conclude therefore, that even before taking into consideration reconstruction efficiency of the leptons, to gain access and sensitivity to the low Δm model points, we must be able to probe low $\Delta R(\ell\ell)$ values, potentially with values less than 0.3. In the next sections we will need to study reconstructed leptons and define isolation criteria that will enable us to retain signal points with close lepton pairs.

As we have seen for $m_{\mu\mu}$ in 6.4.4, reconstruction has an effect on both the shape and overall count of events. We look here at those effects on the $\Delta R(\mu\mu)$ distributions.

When we compare the reconstructed $\Delta R(\mu\mu)$ distributions 6.14 to the generator level ones at 6.12 we see that the main effect of the reconstruction on the $\Delta R(\mu\mu)$ is the overall normalization due to reconstruction efficiency.

6.4.5 Main drivers of sensitivity

We attempt to draw conclusion from this signal distribution studies in regards to the main drivers to the sensitivity of different model points of this analysis, as well as of future analysis that might attempt to expend on this one. In this section we have not looked at SM background
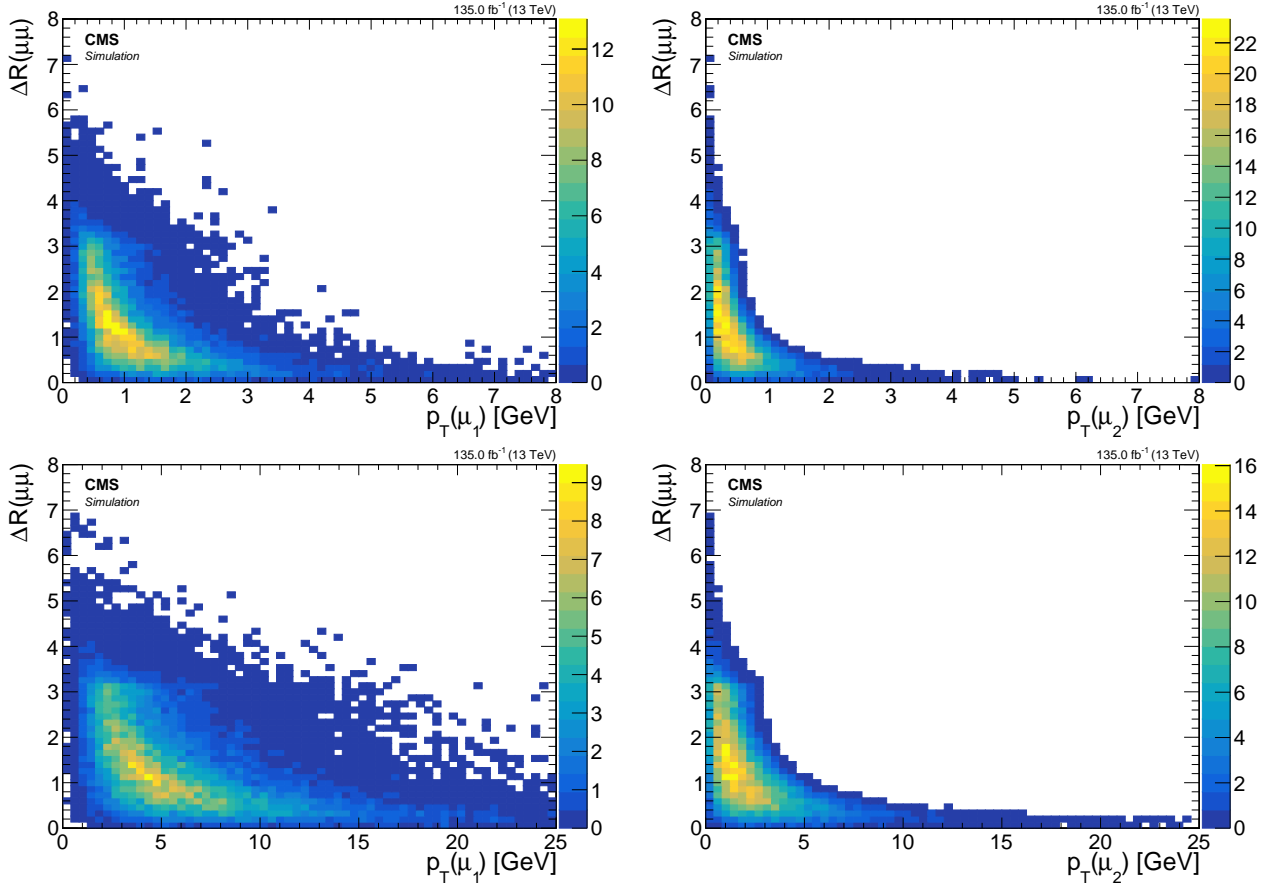
Figure 6.13: Signal $\Delta R(\mu\mu)$ vs. p_T for leading lepton μ_1 (left) and subleading lepton μ_2 (right) for $\Delta m = 1.13\,\text{GeV}$ (top) and $\Delta m = 5.63\,\text{GeV}$ (bottom).
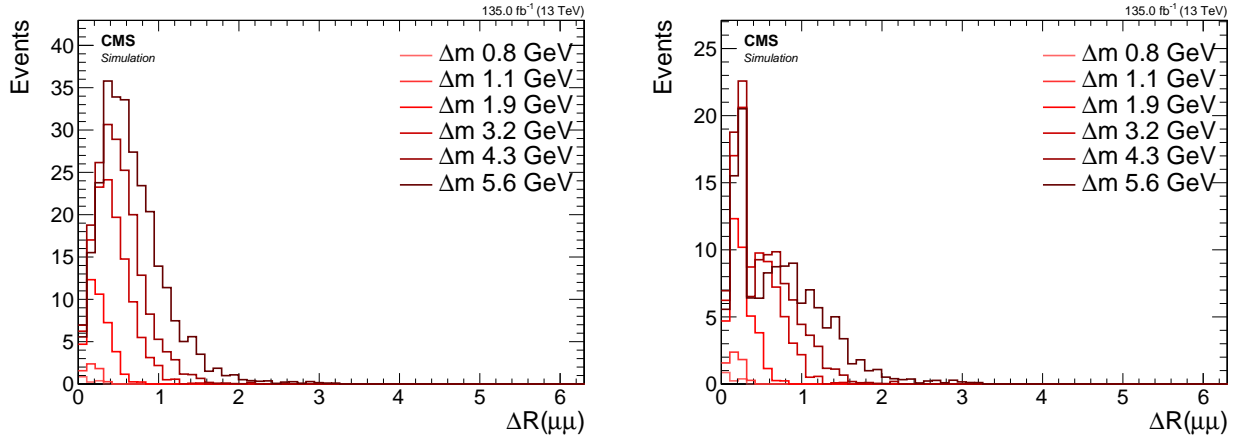

Figure 6.14: Signal reconstructed $\Delta R(\mu\mu)$ with basic analysis selection (left) and additional SOS orthogonality condition (right).

at all. Therefore, it is hard to conclude what effects changing the cuts to E_T^{miss} or other event level observables might have. However, one thing is very clear from examining the dilepton kinematics and that is that to gain access to low Δm model points, one must lower the threshold on of p_T in the selection of the decay leptons and make sure to also be able to probe low ΔR. Another driver of the sensitivity at all Δm model points is the luminosity, since the production cross section drops as a function of the higgsino mass parameter μ.

We will explore in the next sections how we are able to lower the threshold on the muons transverse momentum as well as dealing with collimated leptons that might pose a challenge.

6.5 Search strategy

6.6 Simulated samples

6.6.1 Standard Model simulated samples

6.6.2 Signal simulated samples

6.7 Object definition and selection

We have seen in 5.3 how objects are being reconstructed and identified in our detector. We have also studied the signal signature in 6.4. In this section we devise an object selection in order to obtain as pure as possible sample of objects in regards to our target leptons, while retaining as much signal as possible. As we have seen in 6.5, we are targeting the opposite-charged same-flavor leptons $\ell^+\ell^-$ that result from the $\widetilde{\chi}_2^0$ that decays into a $\widetilde{\chi}_1^0$ via a Z^*, i.e., $\widetilde{\chi}_2^0 \rightarrow \widetilde{\chi}_1^0 \ell^+ \ell^-$. In the following section, we choose to present two choices of Δm^0, namely, $\Delta m^0 = 1.92\,\mathrm{GeV}$ and $\Delta m^0 = 5.63\,\mathrm{GeV}$, i.e., a relatively high Δm^0, and a low one, but not too low as to still be able to have enough electrons surviving the initial reconstruction p_{T} threshold of $5\,\mathrm{GeV}$. We also fix the higgsino parameter on $\mu = 100\,\mathrm{GeV}$.

As was the case in 6.4, the base selection for the following section is requiring at least one jet in the event with $p_{\mathrm{T}} \geq 30\,\mathrm{GeV}$ and $|\eta| < 2.4$. No other selections otherwise. However, unlike 6.4, we do not weight our objects to any luminosity, as we are interested in the proportion between object types. We differentiate between two types of leptons, ones that originate from our targeted decay $\widetilde{\chi}_2^0 \rightarrow \widetilde{\chi}_1^0 \ell^+ \ell^-$, which will be shown in blue, and those that do not, which we refer to as *other*, and are shown in yellow. Leptons that are marked as resulting from the $\widetilde{\chi}_2^0 \rightarrow \widetilde{\chi}_1^0 \ell^+ \ell^-$ decay, which we will refer to as *signal leptons*, are done so by matching a reconstructed lepton to a generator level lepton, which has been checked to have the $\widetilde{\chi}_2^0$ as its parent. Lepton marked as *other*, either has been misreconstructed, misidentified or is a result of hadronisation process in a jet (such as the ISR jet). Our goal here is to select as many blue leptons as possible, while rejecting as many yellow ones as possible. In the following sections, we will refer to *efficiency* as the proportion between the signal leptons passing a selection, divided by the initial number of signal leptons, and to *purity* as the proportion between signal leptons (blue) and the sum of the signal leptons and *other* leptons (yellow). So to rephrase our goal, we are interested in a selection that results in high-efficiency and high-purity. These two quantities can sometimes compete with each other and we have to make compromises.

6.7.1 Electrons

The electrons have an initial reconstruction p_{T} threshold of $5\,\mathrm{GeV}$. The initial working point choice for reconstructed electron is loose (see 5.3). The first distribution we look at in regards to the electrons is their spatial separation from the leading jet in the event, $\Delta R(\jmath_1, \mathrm{e})$.
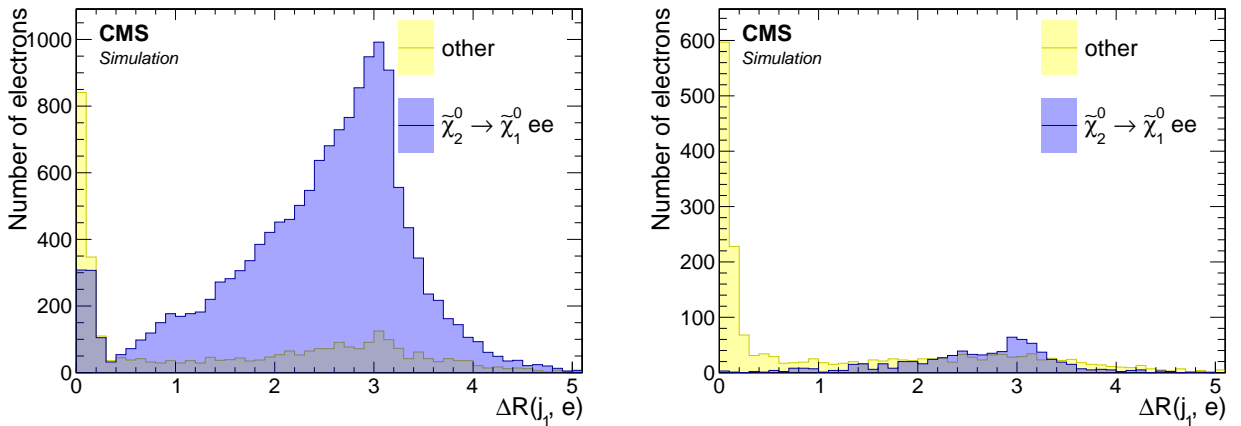

Figure 6.15: Spatial seperation between reconstructed electrons with loose ID and the leading jet $\Delta R(\jmath_1, \mathrm{e})$ for $\Delta m = 5.63\,\mathrm{GeV}$ (left) and $\Delta m = 1.92\,\mathrm{GeV}$ (right).

There are two obvious features we can take from these plots. The first we have explored already in 6.4, namely, that probing lower Δm requires access to low p_{T} leptons, and since we

are limited by a lower threshold of $p_\mathrm{T} \geq 5\,\mathrm{GeV}$ on the electrons, that results in lower signal acceptance as can be seen by the difference between the high Δm and the low one. The second interesting feature that we can see, is that our signal electrons are located mainly outside of the leading jet. That is because the leading jet is usually an ISR jet which boosts the $\widetilde{\chi}_2^0\,\widetilde{\chi}_1^0$ system to away from it (back-to-back). We therefore make a cut $\Delta R(\jmath_1, \mathrm{e}) > 0.4$.

Next we turn into the p_T distributions. We apply the previous cut of $\Delta R(\jmath_1, \mathrm{e}) > 0.4$. As we've already seen in 6.4.4, the p_T distribution depends strongly on Δm. Even though the distributions in 6.4.4 were plotted using generator level muons, the electrons distributions follow the same trend. We therefore need to make a choice about which Δm to favor, i.e., which Δm we want to be more sensitive to, and we choose the lower Δm case. Nonetheless we compare the two choices.
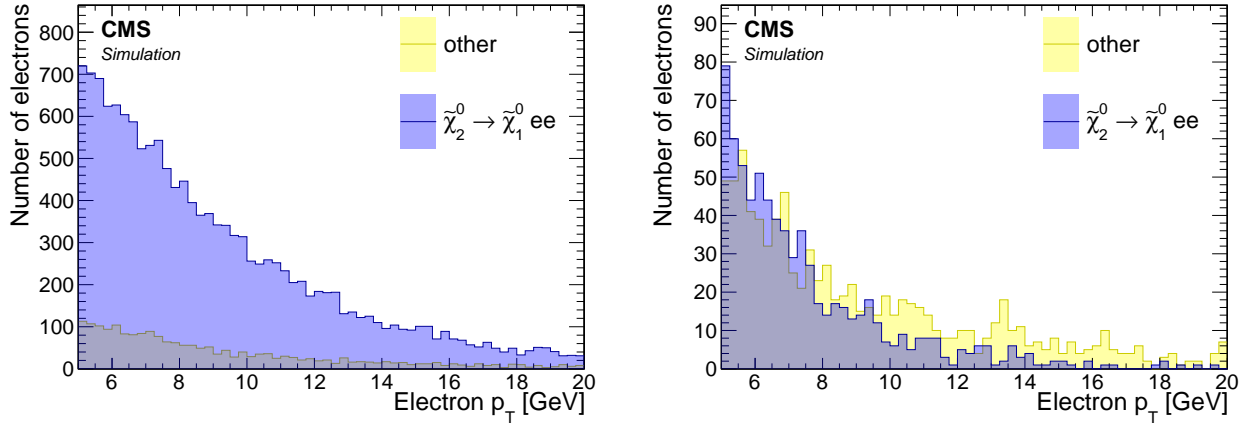
Figure 6.16: p_T distribution of reconstructed electrons with loose ID for $\Delta m = 5.63\,\mathrm{GeV}$ (left) and $\Delta m = 1.92\,\mathrm{GeV}$ (right). Cut of $\Delta R(\jmath_1, \mathrm{e}) > 0.4$ applied.

We can see, as expected, that the p_T distribution of the electrons fall more rapidly for the low Δm case. We observe that there are hardly any electrons surviving above $15\,\mathrm{GeV}$, and therefore we choose to make a cut of $p_\mathrm{T} < 15\,\mathrm{GeV}$.

It interesting to look at the η distribution after the previous cuts to get a better sense of where most of the non-signal electrons are stil coming from.
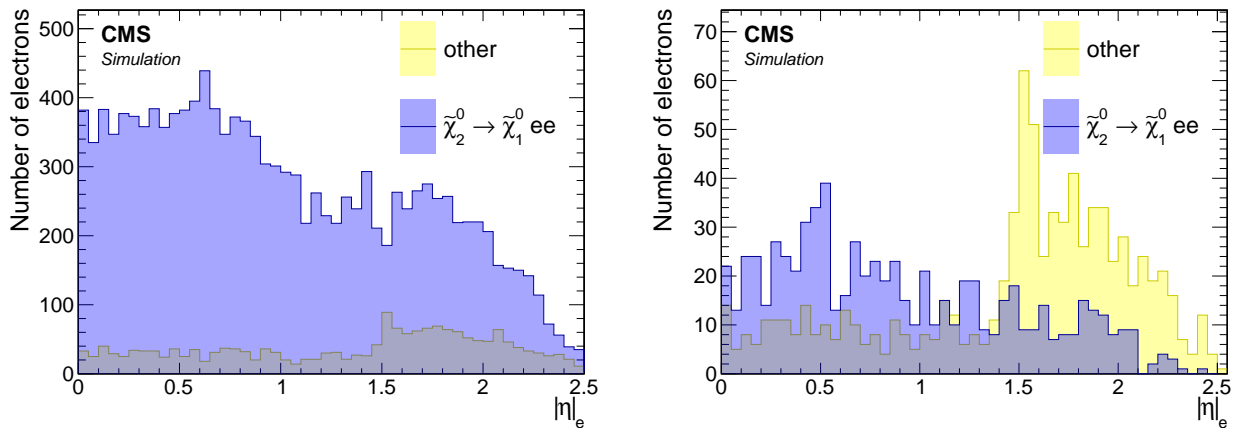

Figure 6.17: $|\eta|$ distribution of reconstructed electrons with loose ID for $\Delta m = 5.63\,\mathrm{GeV}$ (left) and $\Delta m = 1.92\,\mathrm{GeV}$ (right). Cuts of $\Delta R(\jmath_1, \mathrm{e}) > 0.4$ and $p_\mathrm{T} < 15\,\mathrm{GeV}$ are applied.

In the case of $\Delta m = 1.92\,\mathrm{GeV}$, we can clearly see how worse the endcaps of the Electromagnetic Calorimeter (ECAL) are performing in comparison with the barrel ($|\eta| < 1.48$). The

transition is clearly visible through a sharp drop in purity at the transition. It is worse for low-p_T electrons than higher-p_T ones.

We would like to see if requiring a tighter working point for the electron-identification is beneficial. The working point used in the previous distributions is loose. We look turn now to check the effects of requiring either a medium working point, or a tight one. We plot two bins labeled *fail* and *pass*, which correspond to whether the electron passes or failed the identification criteria of a medium or tight working points.
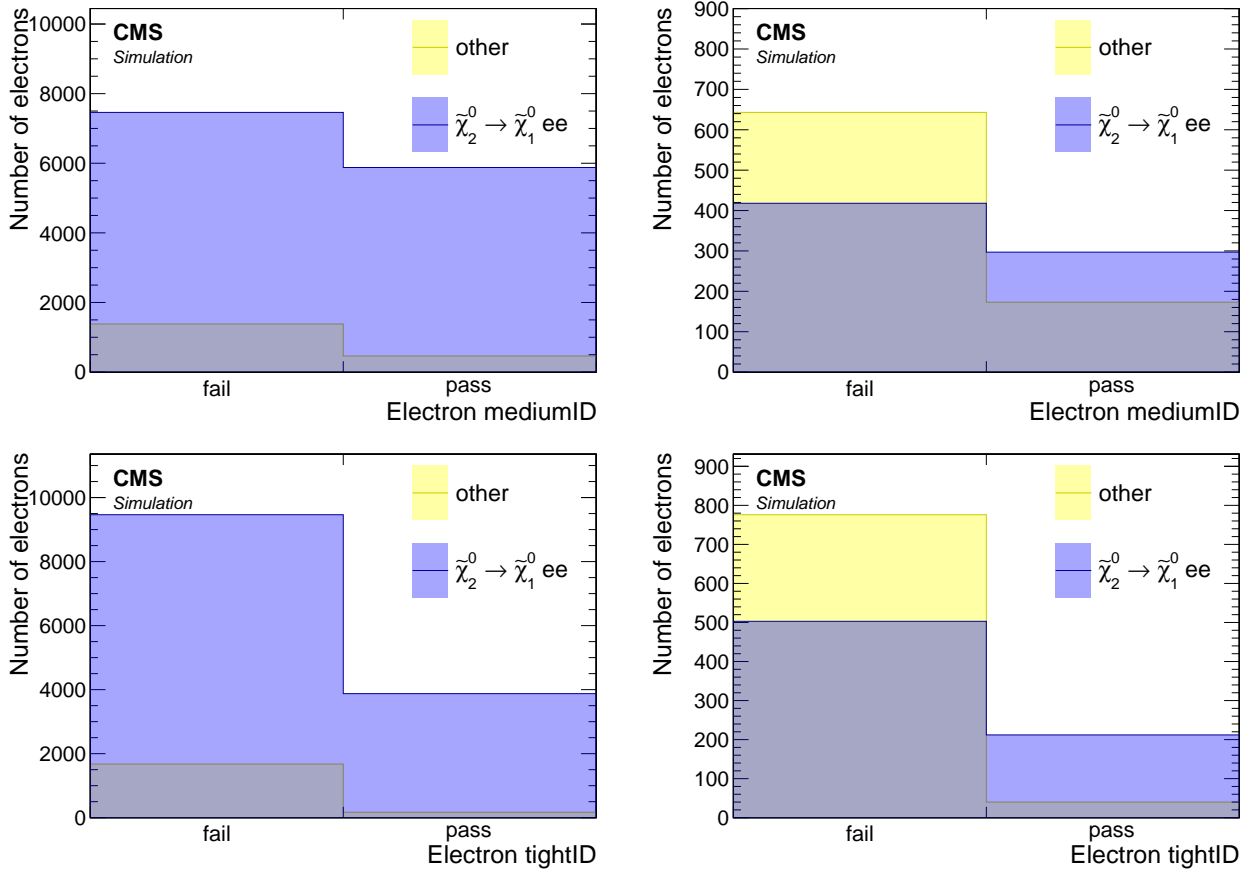
Figure 6.18: Medium (top) and tight (bottom) ID working points distributions of reconstructed electrons for $\Delta m = 5.63\,\mathrm{GeV}$ (left) and $\Delta m = 1.92\,\mathrm{GeV}$ (right). Cuts of $\Delta R(j_1, e) > 0.4$ and $p_\mathrm{T} < 15\,\mathrm{GeV}$ are applied.

Selecting a medium or a tight working point is equivalent to choosing the relevant right *pass* bin (top for medium, bottom for tight), and rejecting the electrons on the left *fail* bin. We see that although we reject considerable amount of non-signal electrons in the low Δm case by picking either a medium or tight working points, we also loose quite a lot of signal electrons as well. In other words, these selections are very not efficient and will result in low signal acceptance. We therefore decide to use a loose working point for the electrons. We will see that we can still purify the electron selection by relying on isolation instead. We fully discuss and describe our jet-isolation in 6.7.6, but here for the sake of completeness we look at its effect on the purity of the electrons. We compare our custom jet-isolation to the standard definition of lepton isolation, which does not take into account the possibility that two electrons can be produced close to each other (small ΔR), as is the case in our signal.

We observe that the standard lepton isolation does not perform well in terms of efficiency for both Δm cases. In contrast, the custom jet-isolation is performing very well in terms of signal electron efficiency while successfully rejecting considerable amount of non-signal electrons, resulting in a purer sample of electrons. We therefore conclude that the choice of the custom
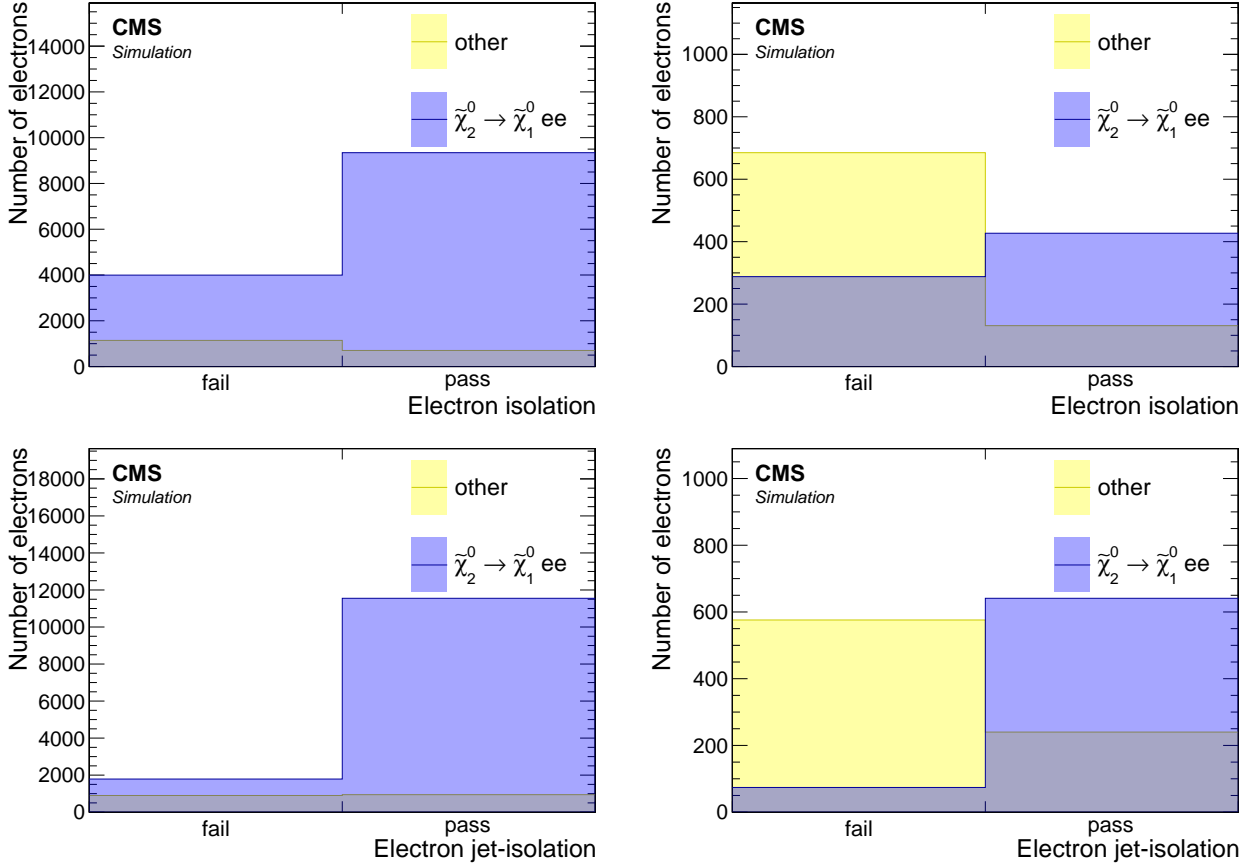
Figure 6.19: Standard isolation (top) and custom jet-isolation (bottom) distributions of reconstructed electrons with loose ID for $\Delta m = 5.63\,\mathrm{GeV}$ (left) and $\Delta m = 1.92\,\mathrm{GeV}$ (right). Cuts of $\Delta R(\jmath_1, e) > 0.4$ and $p_T < 15\,\mathrm{GeV}$ are applied.

jet-isolation is favorable. We can look at how the η distribution is affected by this choice and that will conclude our selection of the electrons.
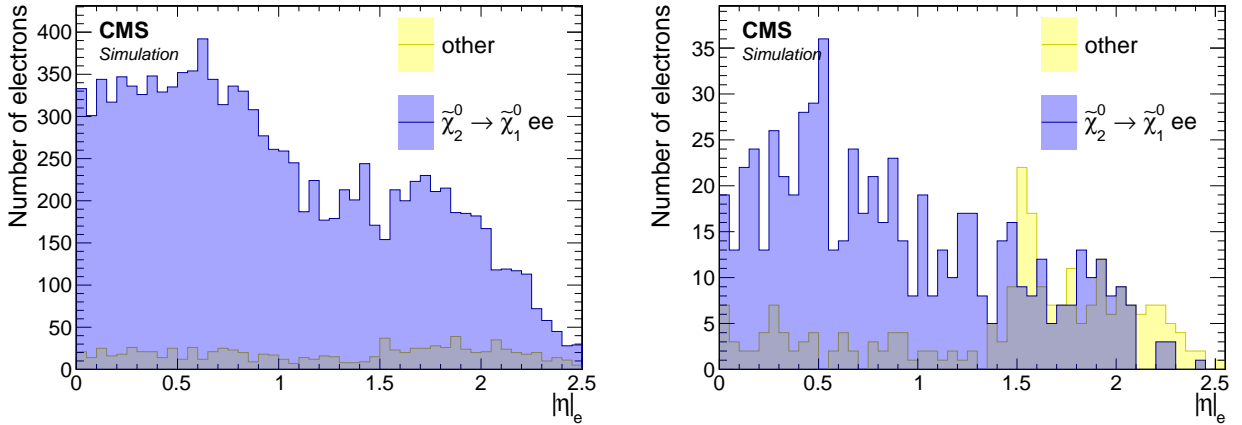

Figure 6.20: $|\eta|$ distribution of reconstructed electrons with loose ID passing jet-isolation for $\Delta m = 5.63\,\mathrm{GeV}$ (left) and $\Delta m = 1.92\,\mathrm{GeV}$ (right). Cuts of $\Delta R(\jmath_1, e) > 0.4$ and $p_T < 15\,\mathrm{GeV}$ are applied.

When we compare distributions 6.20 with 6.17, we can see that our custom jet-isolation has done a good job purifying the electrons selection even further while being efficient in retaining the signal electrons.

We summaries this section with the full selection of the analysis electrons:

- $5 < p_{\mathrm{T}} < 15\,\mathrm{GeV}$
- $|\eta| < 2.5$
- $\Delta R(\jmath_1, \mathrm{e}) > 0.4$
- loose ID working point
- pass jet-isolation

6.7.2 Muons

In contrast to the electrons, we do not have an initial reconstruction p_{T} threshold of $5\,\mathrm{GeV}$. Therefore, we want to explore the possibility of lowering the p_{T} threshold as much as posible. This has been motivated in section 6.4.4, where we saw that the lower Δm we want to probe, the lower p_{T} threshold we have to allow. Like in the electron case, the initial working point choice for reconstructed muon is loose (see 5.3). We follow a similar procedure to the electrons case. The first distribution we look at in regards to the muons is their spatial separation from the leading jet in the event, $\Delta R(\jmath_1, \mu)$. We have seen in 6.7 that the muon endcaps are capable of reconstructing muons with $p_{\mathrm{T}} < 3\,\mathrm{GeV}$ while the barrel cannot. It therefore makes sense to look at a split view of barrel and endcaps for the following distributions.
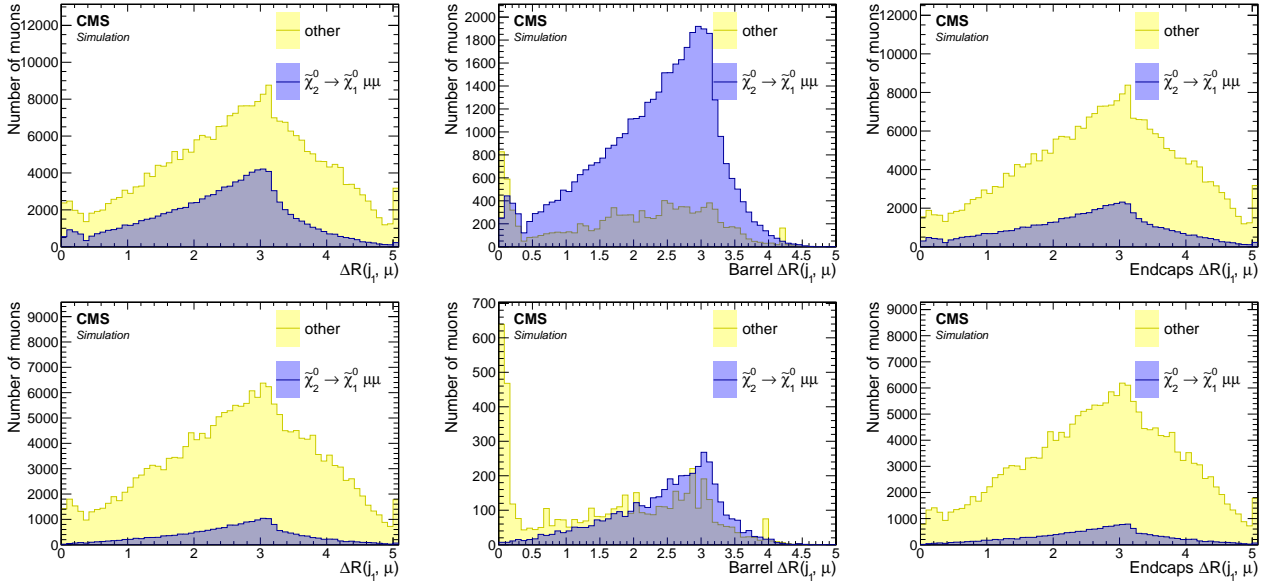
Figure 6.21: Spatial seperation between reconstructed muons with loose ID and the leading jet $\Delta R(\jmath_1, \mu)$ for $\Delta m = 5.63\,\mathrm{GeV}$ (top) and $\Delta m = 1.92\,\mathrm{GeV}$ (bottom) in the inclusive case (left), barrel (middle) and endcaps (right).

Since the muons in the endcaps has lower p_{T} than the muons in the barrel, which is able to reconstruct muons with $p_{\mathrm{T}} > 3\,\mathrm{GeV}$ only, the purity in the endcaps is much lower than the purity in the barrel, and the selection we are constructing here attempts to purify the muons further. Just as in the electrons case, we select muons with $\Delta R(\jmath_1, \mu) > 0.4$, and that selection will apply for the rest of the section.

Next we turn into the p_{T} distributions. We apply the previous cut of $\Delta R(\jmath_1, \mu) > 0.4$. As we've already seen in 6.4.4, the p_{T} and in the electron case, the p_{T} distribution depends strongly on Δm, and we try to favor the low Δm acceptance in order to be more sensitive to it. The p_{T} distributions we see in 6.22 suggest a cut identical to the electron case of $p_{\mathrm{T}} < 15\,\mathrm{GeV}$. It is worth mentioning that the p_{T} of the muons are fed into the training of the Boosted Decision Trees (BDT) for further refinement, and therefore the exact value is being determined here quite loosely. The actual maximum value of the p_{T} of the muons will depend on the BDT cut being used to define the signal region.
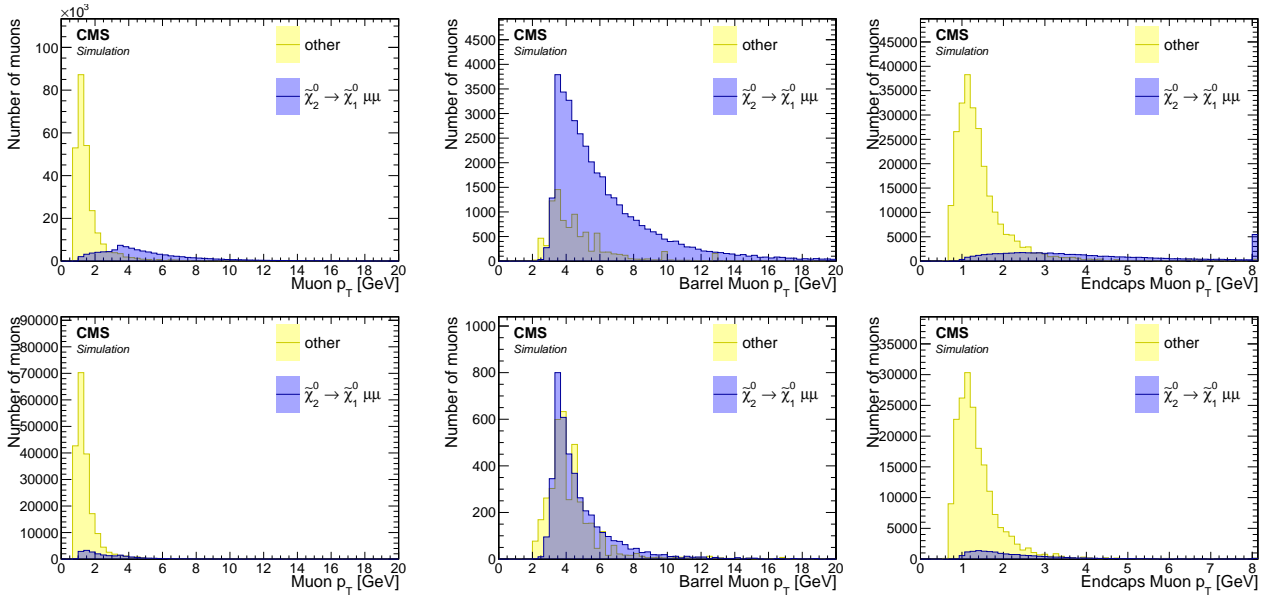
Figure 6.22: Reconstructed muons p_{T} distibution with loose ID for $\Delta m = 5.63\,\mathrm{GeV}$ (top) and $\Delta m = 1.92\,\mathrm{GeV}$ (bottom) in the inclusive case (left), barrel (middle) and endcaps (right). Cuts of $\Delta R(\jmath_1, \mu) > 0.4$ and $p_{\mathrm{T}} < 15\,\mathrm{GeV}$ are applied.

We can see the point being made earlier about the endcaps being able to reconstruct muons with lower p_{T}, and therefore has worse purity than the barrel reiterated here. It must be stressed that worse purity is due to a much higher efficiency, and therefore, as long as we can purify it further, is not necessarily a bad thing. We see however, that the bulk of the non-signal muons populate the region of $p_{\mathrm{T}} < 2\,\mathrm{GeV}$, and the ratio of signal muons to non-signal muons is very low in that region. We therefore make an additional cut of $p_{\mathrm{T}} > 2\,\mathrm{GeV}$. Another way of looking at the effect of this cut is by looking at the $|\eta|$ distribution before and after the p_{T} cut which can be seen in 6.23.

We would like to see if requiring a tighter working point for the muon-identification is beneficial. The working point used in the previous distributions is loose. We look turn now to check the effects of requiring either a medium working point, or a tight one. We plot two bins labeled *fail* and *pass*, which correspond to whether the muon passes or failed the identification criteria of a medium or tight working points.

When we compare the medium working point in 6.24 to the tight working point in 6.25 we can see that the medium working point purifies the muons quite a lot and is very beneficial. However, when we look at the tight working point, we observe that we lose quite a lot of our wanted signal-muons without a significant gain in purity. We therefore choose to use the medium ID working point.

Our custom jet-isolation, which is described fully in 6.7.6, was devised mainly to reject SM background while retaining signal. In the electron case, we have seen in reffig:electrons-selection-isolation that it did a great job in also purifying the electron selection and replaced the need of requiring a tighter identification working point. In the case of the muons, we do rely on the a medium working point to perform this task, but we would like to also see the effects of the isolation on our signal muons. We see in 6.26 that we pay a small price by requiring the isolation, but we increase the sensitivity by rejecting a lot of SM background in the process.

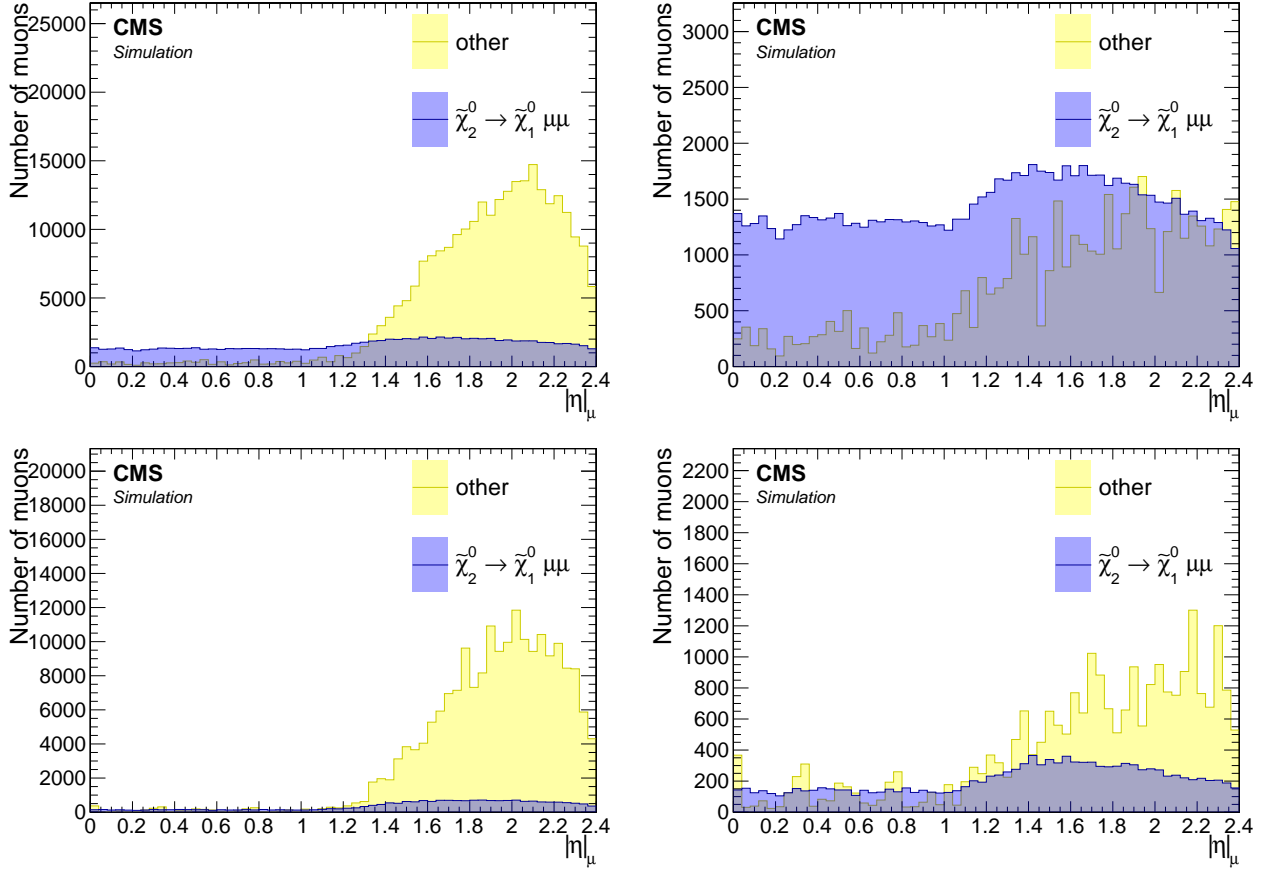We summaries this section with the full selection of the analysis muons:

- $2 < p_{\mathrm{T}} < 15\,\mathrm{GeV}$
- $|\eta| < 2.4$
- $\Delta R(\jmath_1, \mu) > 0.4$

Figure 6.23: $|\eta|$ distribution of reconstructed muons with loose ID for $\Delta m = 5.63\,\mathrm{GeV}$ (top) and $\Delta m = 1.92\,\mathrm{GeV}$ (bottom) without (left) and with (right) $p_T > 2\,\mathrm{GeV}$ cut. Cut of $\Delta R(j_1, \mu) > 0.4$ is also applied.
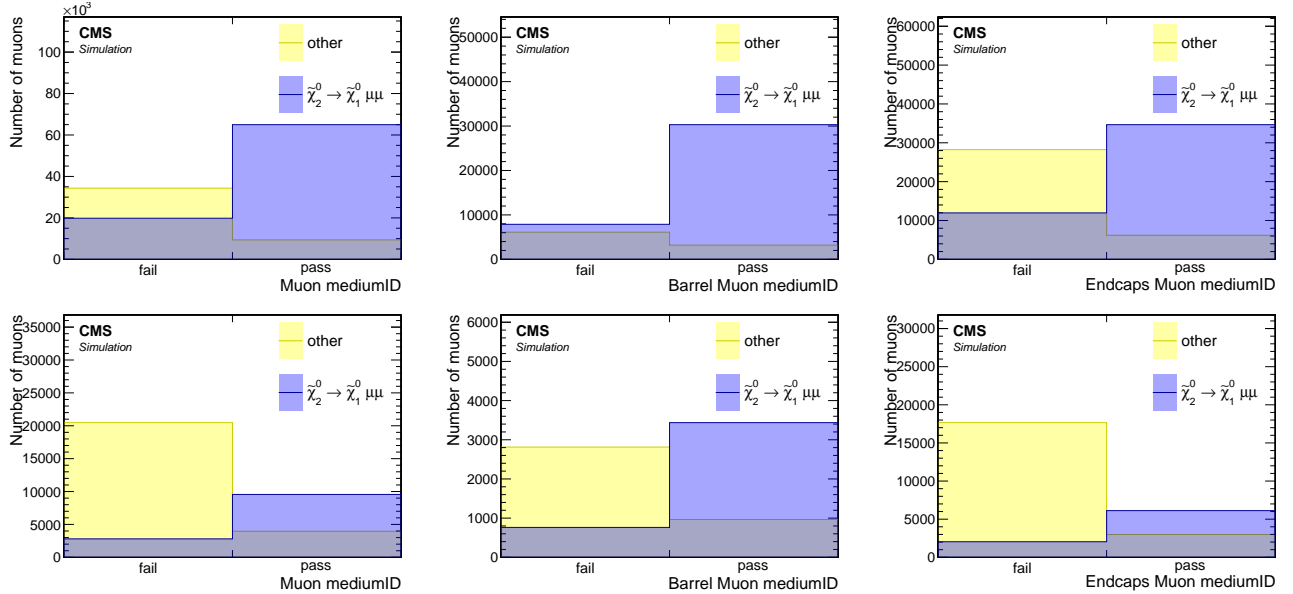

Figure 6.24: Medium ID working point distributions of reconstructed muons for $\Delta m = 5.63\,\mathrm{GeV}$ (top) and $\Delta m = 1.92\,\mathrm{GeV}$ (bottom) in the inclusive p_T case (left), barrel (middle) and endcaps (right). Cuts of $\Delta R(j_1, \mu) > 0.4$, $p_T > 2\,\mathrm{GeV}$ and $p_T < 15\,\mathrm{GeV}$ are applied.

- medium ID working point
- pass jet-isolation
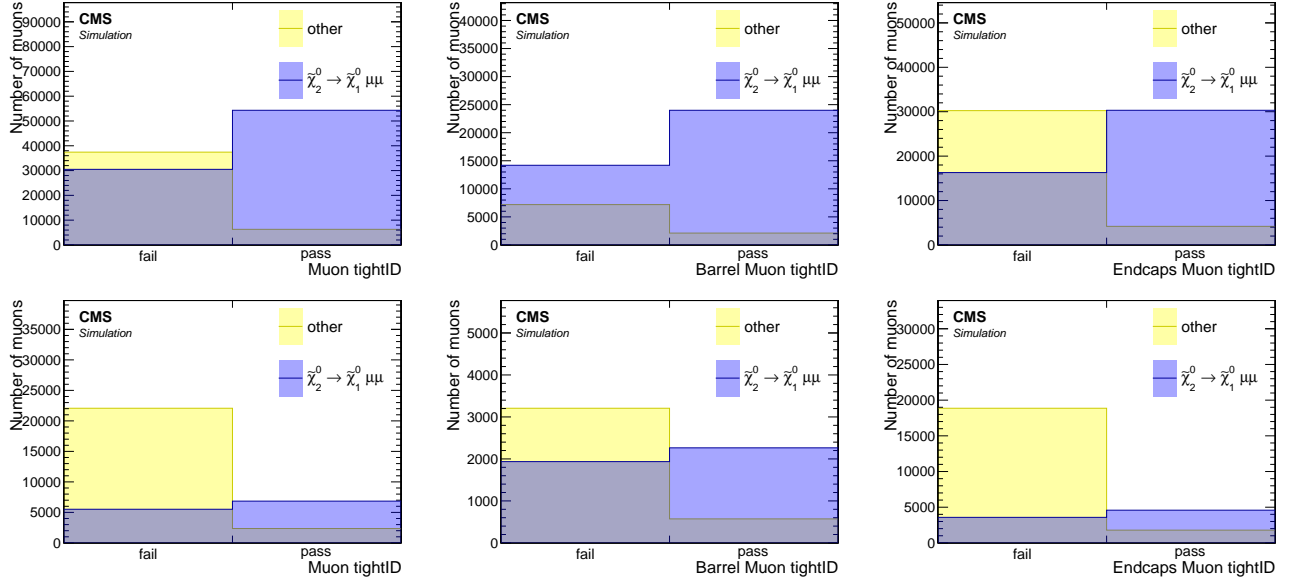
Figure 6.25: Tight ID working point distributions of reconstructed muons for $\Delta m = 5.63\,\text{GeV}$ (top) and $\Delta m = 1.92\,\text{GeV}$ (bottom) in the inclusive p_T case (left), barrel (middle) and endcaps (right). Cuts of $\Delta R(J_1, \mu) > 0.4$, $p_\text{T} > 2\,\text{GeV}$ and $p_\text{T} < 15\,\text{GeV}$ are applied.
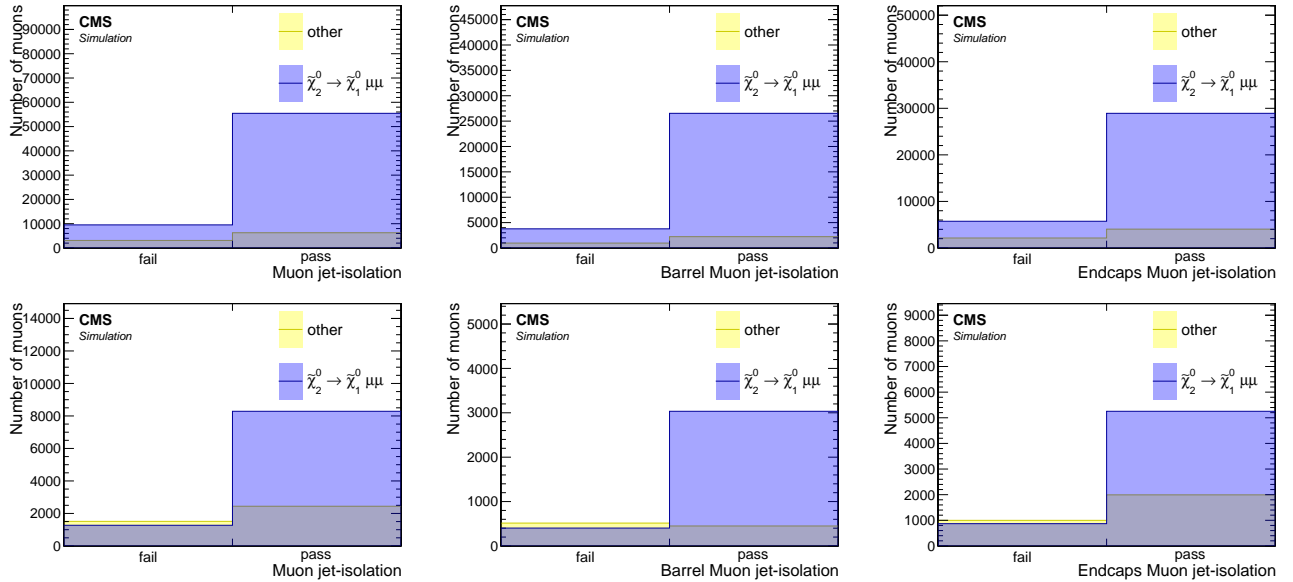
Figure 6.26: Jet-isolation distributions of reconstructed muons with medium ID for $\Delta m = 5.63\,\text{GeV}$ (top) and $\Delta m = 1.92\,\text{GeV}$ (bottom) in the inclusive p_T case (left), barrel (middle) and endcaps (right). Cuts of $\Delta R(J_1, \mu) > 0.4$, $p_\text{T} > 2\,\text{GeV}$ and $p_\text{T} < 15\,\text{GeV}$ are applied.

6.7.3 Scale factors

In 6.7.1 and 6.7.2 we have studied the selection we apply to electrons and muons respectively. We have therewith made a choice about identification working point. We have used simulation exclusively to draw conclusions about the identification efficiency of the leptons. If we rely on Monte Carlo (MC) simulation, that will produce large systematic errors due to imperfections in modeling both the data and the detector response. We therefore wish to measure the identification efficiency in data, in order to correct the simulation's potentially false efficiency rate. *Efficiency* is defined as how probable it is to reconstruct or identify a lepton. For a lepton ℓ the identification efficiency is defined as:

$$\varepsilon_\ell^{\mathrm{ID}} = \frac{N_\ell(\mathrm{ID})}{N_\ell(\mathrm{produced})} \tag{6.1}$$

In MC simulation, the number of leptons produced is the same as the number of leptons generated. In data, one must measure it using a data-driven method. Once the efficiencies have been measured both in simulation and in data, a correction factor named Scale Factor (SF) can be applied to the simulation in order to correct for any discrepancies that might arise. The scale factors are defined as the ratio between the efficiency in data to the efficiency in simulation:

$$\mathrm{SF}_\ell^{\mathrm{ID}} = \frac{\varepsilon_\ell^{\mathrm{ID,Data}}}{\varepsilon_\ell^{\mathrm{ID,MC}}}, \tag{6.2}$$

dropping the superscript ID we get:

$$\mathrm{SF}_\ell = \frac{\varepsilon_\ell^{\mathrm{Data}}}{\varepsilon_\ell^{\mathrm{MC}}}. \tag{6.3}$$

Once the relevant SF have been determined, they are applied for every lepton passing the object selection in the event. The scale factors for loose-ID electrons in our p_{T} range have been measured centrally by the relevant working group and are applied to the selected electrons. As was determined in 6.7.2, our analysis signal muon's lower p_{T} threshold is $2\,\mathrm{GeV}$ which is low. Scale factors for medium ID leptons with $p_{\mathrm{T}} \geq 2\,\mathrm{GeV}$ were computed centrally by the Muon Physics Object Group (POG). The scale factors, however, while matching our muons' p_{T} range and identification working point, were computed by requiring $\Delta R > 0.5$ between the muons [1, 2]. As we have seen in 6.4.4, one of are drivers of the sensitivity is the region of $\Delta R < 0.5$. We would therefore like to validate the scale factors in that region. We would like to show that the efficiencies have no ΔR dependence, and in order to do so, we calculate the efficiencies in different ΔR regions.

In order to measure such efficiency in data, one must identify desired leptons with low and easily reducible fakes. A widely used method to perform such a data-driven task is the Tag & Probe method. In the Tag & Probe method we examine a mass resonance such as Z, J/ψ or Y to select particles of the desired type, and probe the efficiency of a particular selection criterion on those particles. The mass resonance will then decay into two same-flavor opposite charged pair of leptons and will form a peak on top of a background. Since we are interested in measuring the efficiency of low p_{T} muons, we choose to look at dimuon events around the J/ψ mass window. In a dimuon event, we describe one muon as a 'tag' and the other as a 'probe'. The tag muon is selected with a very tight selection which results in very high certainty that the object corresponds to a real muon produced. The probe is given a loose selection, but since it is constrained to be consistent with a product of a J/ψ, it is almost certain that originate from a real muon too. Since the shape of the J/ψ is a peak over a background, the background is easily

removed by fits. The probe is then subjected to cuts or constraints which are used to measure a particular efficiency. As stated, in this study we want to show that the efficiency to identify a muon with medium ID working point from a track has no ΔR depandance. Therefore, the efficiency we are looking for is defined as:

$$\varepsilon_\mu^{\mathrm{ID}} = \frac{N_\mu^{\mathrm{ID}}}{N_t}. \tag{6.4}$$

The probe we are using in the denominator is a track passing a loose selection, while the probe track in the denominator is required to match a medium ID working point muon. The number of objects passing a selection is determined by a fit to data and MC, to measure the corresponding efficiencies in data and MC.

This study is done for year 2016. For the MC, we are using the 2016 samples listed in 6.6.1. For data, we are using a single electron trigger, in order for the tagged muon to be independent from the triggered object. he data set is measured to correspond to $36.02\,\mathrm{fb}^{-1}$ using the BRIL Work Suite [3]. The following trigger paths are used:

- `HLT_Ele27_WPTight_Gsf_v*`,

- `HLT_Ele27_eta2p1_WPLoose_Gsf_v*`,

- `HLT_Ele32_WPTight_Gsf_v*`,

- `HLT_Ele35_WPTight_Gsf_v*`.

We then select an offline loose ID electron with $p_{\mathrm{T}} > 27\,\mathrm{GeV}$ offline. The requirement to select a tag & probe pair are defined in table 6.7.3.

Table 6.3: Selection criteria for Tags and Probes

Tag	Probe
medium ID muon	isolated track
$p_{\mathrm{T}} \geq 5\,\mathrm{GeV}$	$2 \leq p_{\mathrm{T}} \leq 20\,\mathrm{GeV}$ ($p_{\mathrm{T}} \geq 3\,\mathrm{GeV}$ for barrel)
$|\eta| < 2.4$	opposite-sign in invariant mass window $[2.5, 3.5]\,\mathrm{GeV}$

A fit is then performed in an invariant mass window around the J/ψ window of $[2.5, 3.5]\,\mathrm{GeV}$. The signal fit is using a crystal ball function and the continuum is fit with a 6th order polynomial. The fit is repeated twice, where the denominator is done with probe tracks, and the numerator is using medium ID muons that have been matched to said tracks. The ΔR range has been split into 3, and $|\eta|$ of the muons has been split into barrel ($|\eta| < 1.2$) and endcaps ($1.2 < |\eta| < 2.4$). Simulation fits are shown in 6.27 for barrel, and 6.28 for endcaps. Data fits are shown in 6.29 for barrel, and 6.30 for endcaps.

The efficiencies and corresponding scale factors can be seen in 6.31. The scale factors are statistically consistent with unity, and show no discernible ΔR dependence.
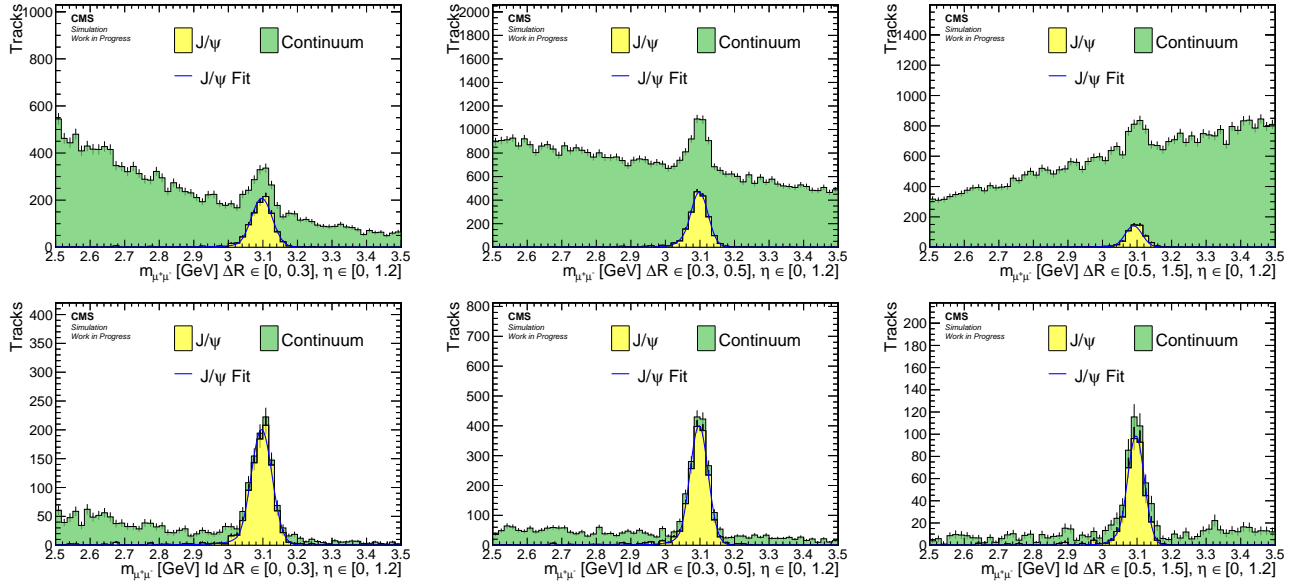
Figure 6.27: Simluation barrel muons fits for denominator (top) and numerator (bottom) for $0 < \Delta R < 0.3$ (left), $0.3 < \Delta R < 0.5$ (center), $0.5 < \Delta R < 1.5$ (right)
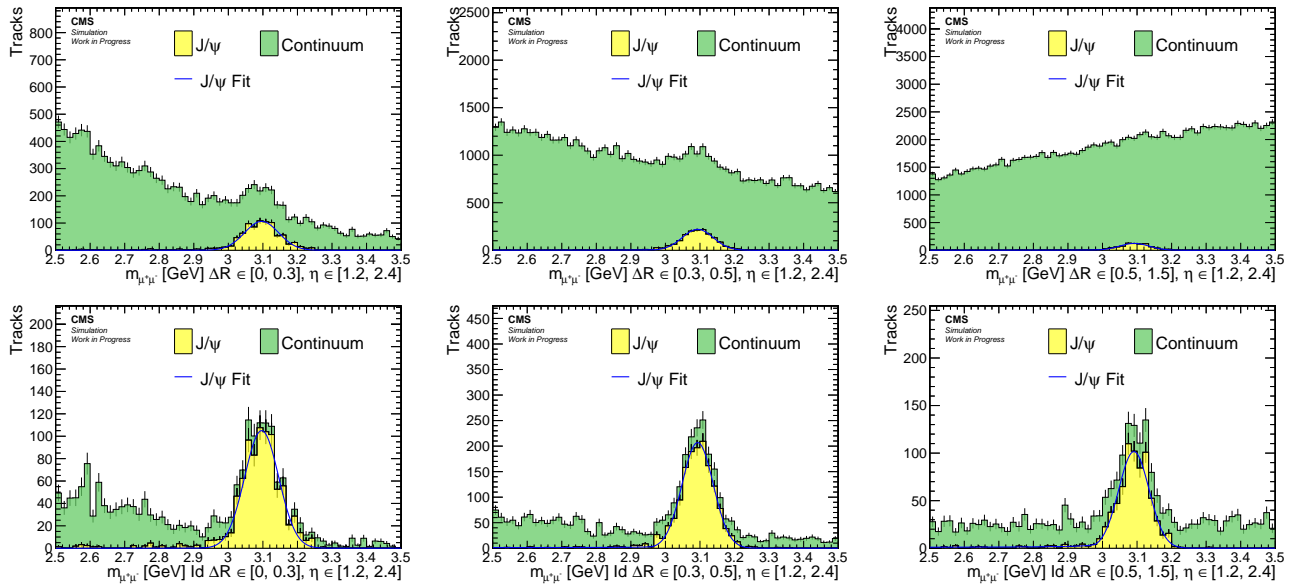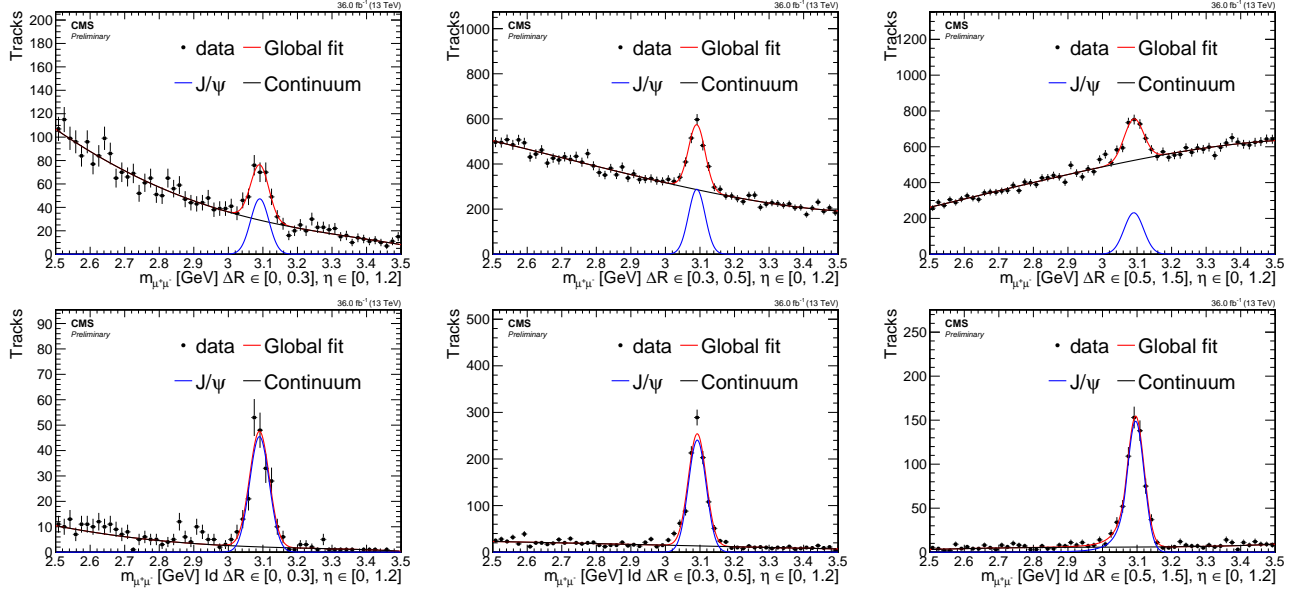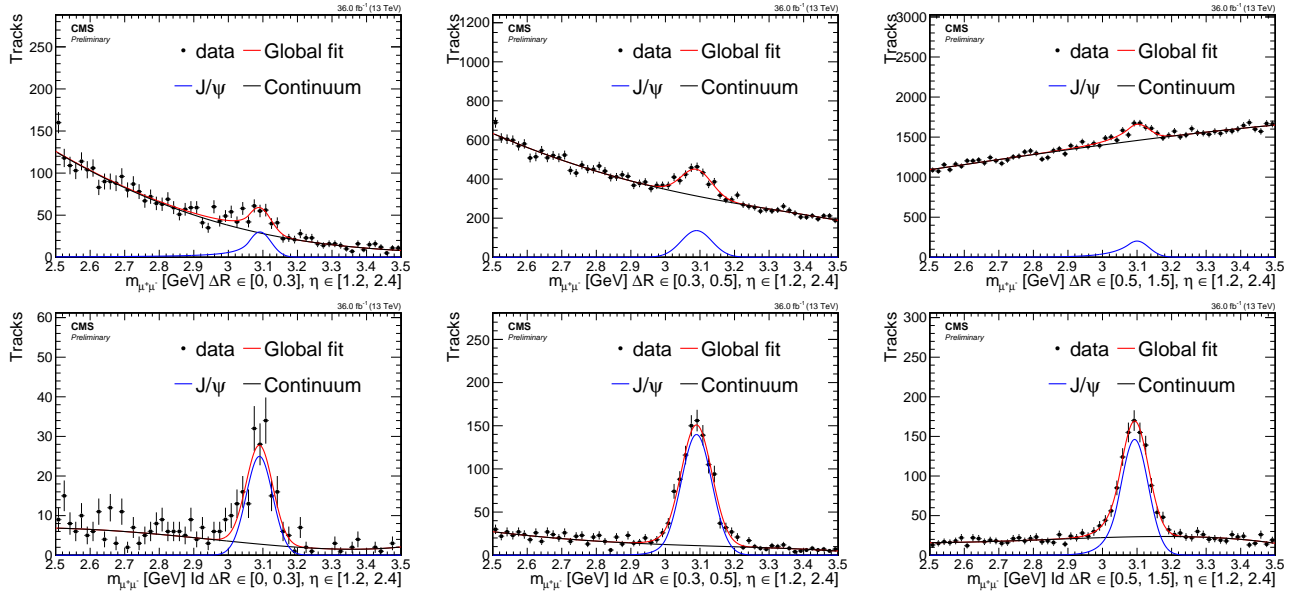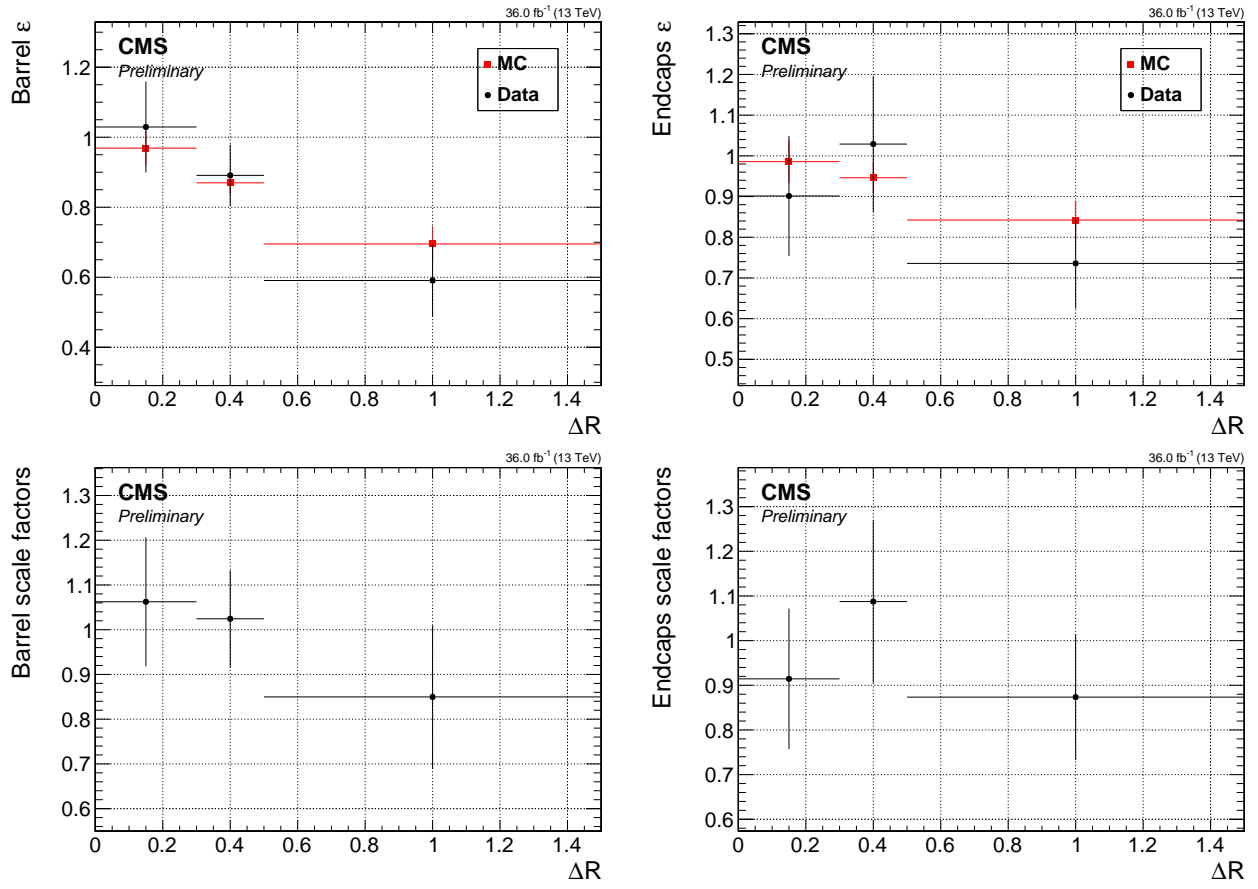

Figure 6.28: Simluation endcaps muons fits for denominator (top) and numerator (bottom) for $0 < \Delta R < 0.3$ (left), $0.3 < \Delta R < 0.5$ (center), $0.5 < \Delta R < 1.5$ (right)

Figure 6.29: Data barrel muons fits for denominator (top) and numerator (bottom) for $0 < \Delta R < 0.3$ (left), $0.3 < \Delta R < 0.5$ (center), $0.5 < \Delta R < 1.5$ (right)

Figure 6.30: Data endcaps muons fits for denominator (top) and numerator (bottom) for $0 < \Delta R < 0.3$ (left), $0.3 < \Delta R < 0.5$ (center), $0.5 < \Delta R < 1.5$ (right)

Figure 6.31: Efficiencies (top) and scale factors (bottom) for barrel muons (left) and endcaps muons (right).

Chapter 7

Jet Isolation and Non-Isolated Background Estimation

7.1 Jet Isolation

7.1.1 Optimisation

7.2 Non-Isolated Background

Chapter 8

Summary

Chapter 9

Latex stuff

9.1 Some examples

9.1.1 Multiline comment

This is a line in introduction.

9.1.2 Fixme note

This is the introduction to the thesis. **FiXme Note: This is a fixme note** **FiXme Note: what** **FiXme Note: WHAT THE HELL** AFTER

9.1.3 Tables

Table 9.1: Table captions are above the table whereas figure captions are below.

Parameter	Value 1	Value 2
s	10.0	20.0
t	20.0	30.0
u	30.0	40.0

9.1.4 Cross References

9.1.4 41 section 9.1.4

9.1.5 Particles

Hello World $\widetilde{\chi}_1^0 \pi \eta_c$ GeV E_T^{miss} hey GeV E_T^{miss} π new one $\widetilde{\chi}_1^0$ $\widetilde{\chi}_1^0$

9.1.6 Citing

[4] SOS analysis

9.1.7 Glossary

Using glossary for compter computer plural form computers upper case first Computer upper case first plural Computers. To use for symbol π

9.1.8   Acronyms

First use of acronym SOS and second SOS. You can reset this and do again Soft-Opposite-Sign (SOS) and second time again SOS. Long version Soft-Opposite-Sign. Full version Soft-Opposite-Sign (SOS). Short version SOS.

List of Corrections

Glossary

computer is a programmable machine that receives input, stores and manipulates data, and provides output in a useful format. 39

$\mathbf{\Delta m}$ mass difference between electroweakinos. If not explicitly said otherwise, it is the mass difference between $\widetilde{\chi}_2^0$ and $\widetilde{\chi}_1^0$, i.e., $\Delta m = \Delta m^0 = m_{\widetilde{\chi}_2^0} - m_{\widetilde{\chi}_1^0}$. 23, 24, 27

$\mathbf{\Delta m^0}$ mass difference between the neutral electroweakinos $\widetilde{\chi}_2^0$ and $\widetilde{\chi}_1^0$, i.e., $\Delta m^0 = m_{\widetilde{\chi}_2^0} - m_{\widetilde{\chi}_1^0}$. 23

$\mathbf{\Delta R}$ separation. 16, 20, 21

$\boldsymbol{\eta}$ pseudorapidity. 20

$\mathbf{E_T^{miss}}$ add description. 12, 13

$\mathbf{H_T^{miss}}$ add description. 12, 13

$\mathbf{m_{\ell\ell}}$ invariant mass. 16–18

neutralino add description. 12, 13

$\boldsymbol{\phi}$ azimuthal angle measured in radians. 20

$\boldsymbol{\pi}$ ratio of circumference of circle to its diameter. 39

$\mathbf{p_T}$ transverse momentum. 12, 13, 15, 16, 20, 23, 24, 27

Acronyms

BDT Boosted Decision Trees. 27

DM Dark Matter. 12

ECAL Electromagnetic Calorimeter. 24

ISR Initial State Radiation. 12, 13, 23, 24

LSP Lightest SUSY Particle. 12

MC Monte Carlo. 31

QCD Quantum Chromodynamics. 12, 13

SF Scale Factor. 31

SM Standard Model. 12, 13, 20, 28

SOS Soft-Opposite-Sign. 18–21, 40

SUSY Supersymmetry. 12

WIMP Weakly Interacting Massive Particle. 12

Bibliography

[1] https://gitlab.cern.ch/cms-muonPOG/MuonReferenceEfficiencies/-/tree/master/ EfficienciesStudies/2016_legacy_rereco/Jpsi.

[2] https://indico.cern.ch/event/791428/contributions/3287172/attachments/ 1781977/2899551/2016LegacyReReco2.pdf.

[3] BRIL Group, "Bril work suite." http://cms-service-lumi.web.cern.ch/cms-service-lumi/brilwsdoc.html, 2017.

[4] **CMS** Collaboration, A. Tumasyan *et al.*, "Search for supersymmetry in final states with two or three soft leptons and missing transverse momentum in proton-proton collisions at $\sqrt{s} = 13$ TeV," *JHEP* **04** (2022) 091, arXiv:2111.06296 [hep-ex].

List of Figures

List of Tables